J. Appl. Comput. Mech., xx(x) (2026) 1-22
DOI: 10.22055/jacm.2026.49250.5837

ISSN: 2383-4536
jacm.scu.ac.ir

Shahid Chamran University of Ahvaz

Journal of Applied and Computational Mechanics

Research Paper

Numerical Investigation of Heat Transfer Enhancement for Finned Double Tube Latent Heat Thermal Energy Storage using Lattice Boltzmann Method

Oussama El Mhamdi[1], Elalami Semma[2], Hamza Faraji[3], Mustapha El Alami[4]

[1] EIGSI, Casablanca, Morocco

[2] Laboratory of Engineering Industrial Management and Innovation, University Hassan 1st, FST Settat, Morocco

[3] Cadi Ayyad University, UCA, National School of Applied Sciences, LaRTID Laboratory, Marrakech, Morocco

[4] Physics Department, LPMAT Laboratory, Faculty of Sciences Ain Chock, Hassan II University, Casablanca, Morocco

Received April 13 2026; Revised August 17 2026; Accepted for publication September 02 2026.
✉ Corresponding author: H. Faraji (hamza.faraji@uca.ac.ma)

Abstract. Latent heat thermal energy storage (LHTES) is a widely employed technique in various practical applications. However, it suffers from the drawback of low conductivity, which significantly impacts the efficiency of both charging and discharging processes. This paper focuses on the numerical study of the thermal performance of a latent heat tube heat exchanger. The investigation involves the consideration of natural convection, and it is conducted using the Lattice Boltzmann method with double population. To take account for the solid/liquid phase change phenomena, the enthalpy method is employed. We investigate the effect of the insertion of conducting fins on the enhancement of thermal transfers within the phase change material (PCM). We explore the influences of control parameters, including the size, number, and thickness of fins, on the duration of the charge and discharge processes within the system. The obtained results show that the presence of natural convection accelerates the melting process by about 25% in the case without fins. The results also disclose that when fins are added, the enhancement of charge-discharge time compared to the case without fins may in some cases reach 80%. In addition, the discharge time is greater than the charge time and the discharge speed depends mainly on the number of fins.

Keywords: Lattice Boltzmann Method; Double tube exchanger; Melting; Solidification; Latent heat storage.

1. Introduction

The industrial field and the needs of the new world impose a sustainable production and supply in term of energy. This sustainable supply is an obligation to ensure the continuity of development and progress reported in various fields and preserving natural resources and reduce the global warming. In the recent years, energy control by storage is becoming a famous kind of energy supply in the development strategies of countries also due to the intermittent behavior of renewable sources. Energy storage can be done by sensible, latent, or thermochemical ways [1, 2]. Phase change materials (PCMs) offer a promising solution for latent heat storage, primarily because of their high storage density and the practically isothermal phase change process [3]. Latent heat storage by PCMs has become an energy trend spreading in many application areas such as thermal management of electronic components, thermal comfort of building, management of agricultural greenhouses [4-8], etc.

PCMs containers come in a variety of geometries and designs, and it all depends on the nature of the desired application. The container characterized by high efficiency, simple geometry and minimal heat loss is the shell-tube model [9, 10]. The use of PCMs as latent storage materials is unfortunately accompanied by the disadvantage of their low thermal conductivity. To solve this problem in shell and tube latent heat energy storage units (LHESU), some studies have investigated the use of multiple heat transfer fluid (HTF) tubes instead of a single one. Esapour et al. [11] conducted a study around the melting of a PCM in a horizontal multi-tube heat exchanger. The used HTF is water, and it flows through the inner and outer tubes while the middle of the exchanger traps the PCM. It was shown that by increasing the number of inner tubes from 1 to 4, the domain occupied by the liquid PCM widens in parallel with a strengthening of the accompanying vortices. This led to a convective heat transfer prevailing in the liquid region and subsequently to a higher melting rate. These results were accompanied by a 29% reduction in melting time. Agyenim et al. [12] experimentally investigated energy storage by PCM in a horizontal heat exchanger. It was proved that the phase change process in the multi-tube heat exchanger is dominated by convection more than by thermal conduction. Furthermore, the appearance of multiple flow cells clearly shows the influence of natural convection on the shape of the melting front. In a similar vein, Joybari et al. [13] compared the thermal behavior during the melting of a PCM (RT-60) in a single-tube and

Published online: September 04 2026

multi-tube heat exchanger. The case studied is for a five-tube exchanger. It was shown that the use of a multi-tube heat exchanger instead of a single-tube heat exchanger improves the convection effects and subsequently accelerates the melting process of the PCM. In this case, the melting time was reduced by 73.6%. Kousha et al. [14] also proved all these results in an experimental study. Furthermore, it was shown that by increasing the number of tubes, the average Nusselt number decreases. This could be attributed to the inhibition of the upper tubes against the movement of the molten PCM.

There are other methods for enhancing heat transfer in PCMs. On the one hand, there is the insertion of solid nanoparticles into the PCM [15-18]. On the other hand, the integration of metal fins within the domain occupied by the PCM is also a promising solution for the improvement of heat transfer. Adopting this improvement strategy, Al-Mudhafar et al. [19] numerically investigated the improvement of the thermal performance of a shell and tube heat exchanger by adding metal fins within the PCM. The main interest of this study was the acceleration of the PCM melting process. The found results showed that the total melting time of the PCM was reduced by 33% by the insertion of fins compared to the case without fins. In addition, the geometry of the fins has a major influence on the progress of this melting process. Xu et al. [20] proposed a strategy for heat transfer enhancement within a shell and tube heat exchanger. This strategy was based on the integration of metal fins within the base PCM. However, it was found that the addition of fins significantly reduced the natural convection of liquid PCMs. In the presence of metal fins, the total melting time was reduced by 71% compared to the base case where there are no fins. Different fin arrangements were analyzed to determine the optimal configuration that guarantees the best heat transfer rate improvement. In the same sense, Yagci et al. [21] analyzed the thermal response of a PCM during its melting in the presence of fins. These latters were added as thermal performance enhancers to the storage system. The parameters investigated were the fin geometry, the edge length ratio (length of the top edge / length of the bottom edge) and the temperature of the inlet fluid. The found results showed that by adding a metal fin, the recirculation was intensified in the lower half region of the annulus. In addition, the melting time was reduced by 21% by decreasing the fin edge length ratio from 1 to 0. Dekhil et al. [22] introduced fins, as surface extensions, in a horizontal storage unit. The results of this numerical study showed that the use of fins significantly increases the solidification and melting rates and therefore the charging and discharging processes. This increase is more significant in the case where the fins were longitudinal.

Based on the literature review and to the best of our knowledge, there is not enough work that focuses on modeling the melting process of PCMs for latent thermal energy storage in vertical double tube heat exchangers with presence of fins. The main originality of this study lies in the fact that it combines the analysis of the thermal response of a PCM during the melting and solidification processes in the presence of metallic fins as surface extensions in order to improve its thermo-physical properties. In addition, it should be noted that this work announces that the novelty lies in the use of the Lattice Boltzmann LBM method to model the thermal and hydrodynamic phenomena and that the enthalpy-porosity method is adopted for phase change modeling. This will eventually help in the development of design strategies for thermal storage systems such as solar energy storage systems.

2. Model Description

2.1. Physical model

The heat exchanger's geometrical configuration is shown in Fig. 1(a). The heat transfer process involves the circulation of a Heat Transfer Fluid (HTF) within the inner tube, wherein it flows downwards during the charging phase and upwards during the discharging phase. Surrounding the inner tube, the outer tube contains a Phase Change Material (PCM). The outer cavity has metal fins for better heat melting through the PCM as illustrated in Fig. 1(b) that shows a real case of utilization.

2.2. Mathematical model

The phase change process is investigated using the total enthalpy model, where the PCM, in its liquid state, is considered to be Newtonian and incompressible. The model considers the PCM to possess constant thermodynamic properties, except for the density variation incorporated in the buoyancy term, in which the Boussinesq approximation is adopted and the buoyancy term can be written as: $F = g\beta(T - T_{ref})$; where g and β are the gravitational acceleration and the thermal expansion coefficient. T and T_{ref} refer to the temperature and the reference temperature, respectively.

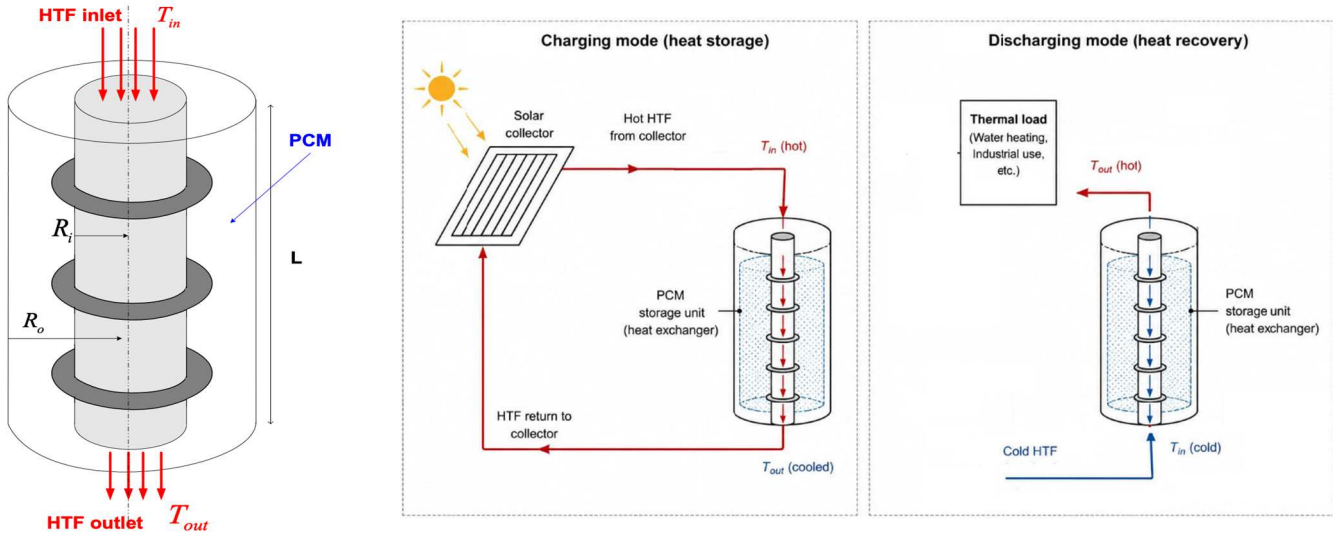

Fig. 1. Heat exchanger configuration, (a) Simplified model, (b) Schematic configuration of a solar thermal energy storage system with a PCM heat exchanger.

Considering the hypotheses already mentioned, the continuity and momentum equations for the PCM region and HTF zone, are given as [23]:

$$\frac{\partial u_r}{\partial r}+\frac{u_r}{r}+\frac{\partial u_z}{\partial z}=0 \tag{1}$$

$$\rho\frac{\partial u_z}{\partial t}+\rho u_r\frac{\partial u_z}{\partial r}+\rho u_z\frac{\partial u_z}{\partial z}=-\frac{\partial p}{\partial r}+\mu\left(\frac{\partial^2 u_z}{\partial r^2}+\frac{\partial u_z}{r\partial r}+\frac{\partial^2 u_z}{\partial z^2}\right)+\rho g\beta(T-T_{ref}) \tag{2}$$

$$\rho\frac{\partial u_r}{\partial t}+\rho u_r\frac{\partial u_r}{\partial r}+\rho u_z\frac{\partial u_r}{\partial z}=-\frac{\partial p}{\partial z}+\mu\left(\frac{\partial^2 u_r}{\partial r^2}+\frac{\partial u_r}{r\partial r}+\frac{\partial^2 u_r}{\partial z^2}-\frac{u_r}{r^2}\right) \tag{3}$$

where μ is the fluid viscosity, u_r and u_z are the partial velocities in r and z directions, and P is the pressure. The total enthalpy-based energy governing equation is:

$$\frac{\partial \rho H}{\partial t}+u_r\frac{\partial \rho C_pT}{\partial r}+u_z\frac{\partial \rho C_pT}{\partial z}=\frac{1}{r}\frac{\partial}{\partial r}\left(rk\frac{\partial T}{\partial r}\right)+\frac{\partial}{\partial z}\left(rk\frac{\partial T}{\partial z}\right) \tag{4}$$

where C_p and k are the specific heat and the thermal conductivity, respectively. H is the sum of the sensible enthalpy and the latent enthalpy:

$$H=C_pT+f_lL_f \tag{5}$$

where f_l is the liquid phase volume fraction and L_f is the latent heat. In the solid fin, the energy equation can be described as:

$$\rho_{fin}\frac{\partial}{\partial t}(C_{p,fin}T)=\frac{1}{r}\frac{\partial}{\partial r}\left(rk_{fin}\frac{\partial T}{\partial r}\right)+\frac{\partial}{\partial z}\left(rk_{fin}\frac{\partial T}{\partial z}\right) \tag{6}$$

- Initial and boundary conditions:

The whole computational domain is initially at thermal equilibrium with the dimensionless temperature of T_f:

$$T_0(r,z,t=0)=T_f \tag{7}$$

- Dynamic boundary conditions:

For HTF:

$$\begin{aligned} &u_r=0,\ u_z=V_{in} \text{ for } 0\le r\le R_i \text{ and } z=L\\ &u_r=0,\ u_z=0 \text{ for } r=R_i \text{ and } 0\le z\le L\\ &u_r=0,\ \frac{\partial u_z}{\partial r}=0 \text{ for } r=0 \text{ and } 0\le z\le L\\ &u_r=0,\ \frac{\partial u_z}{\partial z}=0 \text{ for } 0\le r\le R_i \text{ and } z=0 \end{aligned} \tag{8}$$

For PCM

$$\begin{aligned} &u_r=0, u_z=0 \text{ for } r=R_i \text{ and } 0\le z\le L\\ &u_r=0, u_z=0 \text{ for } R_i\le r\le R_0 \text{ and } z=0\\ &u_r=0, u_z=0 \text{ for } R_i\le r\le R_0 \text{ and } z=L \end{aligned} \tag{9}$$

- Thermal boundary conditions:

For HTF:

$$\begin{aligned} &T=T_{in} \text{ for } 0\le r\le R_i \text{ and } z=L\\ &\frac{\partial T}{\partial r}=0 \text{ for } r=0 \text{ and } 0\le z\le L \end{aligned} \tag{10}$$

For PCM:

$$\begin{aligned} &\frac{\partial T}{\partial z}=0 \text{ for } R_i\le r\le R_o \text{ and } z=L\\ &\frac{\partial T}{\partial z}=0 \text{ for } R_i\le r\le R_o \text{ and } z=0\\ &\frac{\partial T}{\partial r}=0 \text{ for } r=R_o \text{ and } 0\le z\le L \end{aligned} \tag{11}$$

The contact between the fluid and the solid fins is designated here by “s”. The boundary conditions are given by the continuity condition of temperature and thermal flow:

$$T_{PCM}=T_s \tag{12}$$

$$\mathrm{n}.\left(-k\nabla T+\rho C_p \mathrm{u}T\right)_{PCM}=\mathrm{n}.\left(-k\nabla T\right)_s \tag{13}$$

The system is controlled by a group of dimensionless numbers including Prandtl number of the HTF, Prandtl number of the PCM, Rayleigh number and Stefan number of the PCM, the ratio of the thermal conductivities of fins, the fluid and the PCM, and the ratio of specific heat of fins and the PCM:

- Prandtl Numbers of HTF and PCM:

$$\mathrm{P}_{r,HTF}=\frac{\upsilon_{HTF}}{\alpha_{HTF}} \tag{14}$$

$$\mathrm{P}_{r,PCM}=\frac{\upsilon_{PCM}}{\alpha_{PCM}} \tag{15}$$

- Rayleigh number:

$$Ra=\frac{g\beta\Delta T\mathrm{L}^3}{\alpha_{PCM}\upsilon_{PCM}} \tag{16}$$

- Stefan number of the PCM:

$$Ste=\frac{C_{p,PCM}\Delta T}{L_f} \tag{17}$$

- Ratio of conductivities of the fins and PCM:

$$\kappa_s=\frac{\mathrm{k}_s}{\mathrm{k}_{PCM}} \tag{18}$$

- Ratio of conductivities of the fluid and the PCM:

$$\kappa_{HTF}=\frac{\mathrm{k}_{HTF}}{\mathrm{k}_{PCM}} \tag{19}$$

- Ratio of specific heats of the fins and the PCM:

$$c_s=\frac{(\rho C_p)_s}{(\rho C_p)_{PCM}} \tag{20}$$

- Ratio of specific heats of the fluid and the PCM:

$$c_{HTF}=\frac{(\rho C_p)_{HTF}}{(\rho C_p)_{PCM}} \tag{21}$$

- Fourier number:

$$Fo=\frac{\alpha_{PCM}\mathrm{t}}{L^2} \tag{22}$$

- Reynolds number of the HTF:

$$Re_{HTF}=\frac{2\mathrm{V}_{in}\mathrm{R}_1}{\upsilon_{HTF}} \tag{23}$$

2.3. Numerical method

Recently, there has been significant interest in utilizing the Lattice Boltzmann method to simulate axisymmetric flows. Remarkably, axisymmetric flows can be efficiently simulated using a 3D Lattice Boltzmann model, even though they inherently possess an axisymmetric property. However, by directly employing a 3D model, the full advantage of this axisymmetric property is not fully exploited, as a 3D axisymmetric flow can be equivalently reduced to a quasi-two-dimensional 2D problem.

This study develops a double-distribution-function thermal lattice Boltzmann model for the simulation of axisymmetric flow coupled with heat transfer and phase change phenomena. The model employs two sets of distribution functions: one for density and velocity, based on the general Navier–Stokes model, and another for temperature, specifically modified to address the conservation of total enthalpy energy. To facilitate the simulation of two-dimensional fluid flow, the D2Q9 lattice is utilized, while D2Q5 lattice is adopted to handle the temperature field in heat transfer aspects of the problem.

To cancel the velocity in the solid phase, we adopt the technique developed by Huang et al. [24, 25] using the schemes of submerged solids by modifying the Lattice Boltzmann equations according to the following expression:

$$f_i(x+e_i\delta t,t+\delta t)=f_i(x,t)+\frac{1-B}{\tau_f}\left(f_i(x,t)-f_i^{eq}(x,t)\right)+B\Omega_i^s+\frac{\delta t}{2}\left(F_i(x,t)+F_i(x+e_i\delta t,t+\delta t)\right) \tag{24}$$

where f_i is the momentum distribution function, f_i^{eq} is the momentum equilibrium distribution function, F_i is the discrete forcing term, τ_f is the relaxation time and B is a weighting coefficient related to the liquid fraction and the dimensionless relaxation time:

$$B=(1-f_l)\frac{(\tau_f-0.5)}{\tau_f+f_l-0.5} \tag{25}$$

where Ω_i^s denotes the collision term based on the bounce back principle of the non-equilibrium term given by:

$$\Omega_i^s=f_{\bar{i}}(x,t)-f_{\bar{i}}^{eq}(x,t)-f_i(x,t)+f_i^{eq}(x,t) \tag{26}$$

with $\bar{i}$ is the opposite direction to i. The expression of f_i^{eq} and F_i can be, respectively, written as:

$$f_i^{eq}(x,t)=r\rho\omega_i\left(1+\frac{e_i.u}{c_s^2}+\frac{(e_i.u)^2}{2c_s^4}-\frac{u.u}{2c_s^2}\right) \tag{27}$$

$$F_i(x,t)=\rho\omega_i\left[\left(c_s^2-\frac{2}{r}\upsilon u_r\right)\frac{e_{ir}}{c_s^2}+\frac{u.e_i}{c_s^2}e_{ir}-u_r\right]+r\rho\omega_i\frac{(e_i-u).a}{c_s^2} \tag{28}$$

with $u = (u_r, u_z)$ the velocity vector with the radial and vertical components and ω_i the weighting coefficients of the D2Q9 model namely:

$$\omega_i=\begin{cases}\frac{4}{9} & i=0\\ \frac{1}{9} & i=1,2,3,4\\ \frac{1}{36} & i=5,6,7,8\end{cases} \tag{29}$$

The velocity vector of particles for D2Q9 model is defined by:

$$c_i=\begin{cases}(0,0) & i=0\\ \left(\cos\left[\frac{(i-1)\pi}{2}\right],\sin\left[\frac{(i-1)\pi}{2}\right]\right)c & i=1,2,3,4\\ \left(\cos\left[\frac{(2i-9)\pi}{4}\right],\sin\frac{(2i-9)\pi}{4}\right)\sqrt{2}c & i=5,6,7,8\end{cases} \tag{30}$$

where $c = \delta x / \delta t$ is the particle streaming speed on the lattice taken as $c = 1$. δx and δt denote the constant lattice space and the time step, respectively. c_s is the lattice sound speed with a value $c_s^2 = 1/3$. The density and velocity in macro scale are, respectively, obtained by:

$$\rho=\frac{1}{r}\sum_i f_i \tag{31}$$

$$u=\frac{1}{\rho r}\sum_i e_i f_i \tag{32}$$

The relaxation time τ_f is associated with the kinematic viscosity by:

$$\upsilon=(\tau_f-0.5)\delta t c_s^2 \tag{33}$$

The D2Q5 model is adopted to simulate the total enthalpy field. The evolution equation of the distribution function is expressed by:

$$g_i(x+e_i\delta t,t+\delta t)=g_i(x,t)+\frac{1}{\tau_g}\left(g_i(x,t)-g_i^{eq}(x,t)\right)+\frac{\delta t}{2}\left(G_i(x+e_i\delta t,t+\delta t)+G_i(x,t)\right) \tag{34}$$

where g_i is the energy distribution function, g_i^{eq} is the equilibrium energy distribution function, G_i is the discrete forcing term and τ_g is the dimensionless single relaxation time for heat transfer. Here, the equilibrium distribution function is given by the scheme developed by Huang and Wu [25]:

$$g_i^{eq}=\begin{cases}r\rho H-r\rho C_{p0}T+r\lambda_i\rho C_pT\left(\frac{\rho_0C_{p0}}{\rho C_p}-\frac{u^2}{2c_s^2}\right) & i=0\\ r\lambda_i\rho C_pT\left(\frac{\rho_0C_{p0}}{\rho C_p}+\frac{e_iu}{c_s^2}+\frac{(e_iu)^2}{c_s^4}-\frac{u^2}{2c_s^2}\right) & i\neq 0\end{cases} \tag{35}$$

where C_{p0} is a reference heat capacity, which takes a constant value over the entire space lattice. The discrete forcing term is given by:

$$G_i = \rho \lambda_i C_p e_{ir}$$

where λ_i are the weighting coefficients of the D2Q5 model and are namely:

$$\lambda_i = \begin{cases} \frac{1}{3} & i = 0 \\ \frac{1}{6} & i = 1,2,3,4 \end{cases} \tag{36}$$

The total enthalpy H, the liquid fraction f_l and the temperature T are calculated as [24, 26]:

$$H = \frac{1}{\rho r} \sum_0^4 g_i \tag{37}$$

$$f_l = \begin{cases} 0 & H < H_s \\ \frac{H - H_s}{H_l - H_s} & H_s \le H \le H_l \\ 1 & H_l < H \end{cases} \tag{38}$$

$$T = \begin{cases} \frac{H}{C_p} & T < T_s \\ \frac{H - H_s}{H_l - H_s} T_l + \frac{H_l - H}{H_l - H_s} T_s & T_s \le T \le T_l \\ T_l + \frac{H - H_l}{C_p} & T_l < T \end{cases} \tag{39}$$

with T_l and T_s are the liquidus and solidus temperatures. $H_l = \rho C_p T_l + L_f$ and $H_s = \rho C_p T_s$ are the total enthalpies corresponding to the liquidus and solidus temperatures. L_f is the latent heat of the PCM. The thermal relaxation time of the different zones is related to the conductivity with the following relation:

$$\tau_g = \begin{cases} 3\frac{k_{PCM}}{\rho_0 C_{p0}} + 0.5 & \text{in the PCM} \\ 3\frac{k_{fins}}{\rho_0 C_{p0}} + 0.5 & \text{in the fin} \\ 3\frac{k_{HTF}}{\rho_0 C_{p0}} + 0.5 & \text{in the HTF} \end{cases} \tag{40}$$

The heat transfer rate can be quantitatively examined by the average Nusselt number on the inner cylinder wall:

$$Nu = -\frac{R_i}{L\Delta T} \int_0^L \left. \frac{\partial T}{\partial r} \right|_{r=R_i} dz \tag{41}$$

2.4. Numerical calculation and validation

- Hagen-Poiseuille flow

We consider in this part an infinite cylindrical pipe. For the simulation of this type of flow, we consider a cylindrical channel with periodic conditions at the inlet and the outlet which means that the outlet is connected to the inlet. The flow is controlled by the pressure between the two ends of the channel. The computational domain is $0 \le r \le R$ and $0 \le z \le L$, with $r = 0$ on the axis of symmetry and the solid wall is located at $r = R$. The boundary conditions of the fluid variables are:

$$\begin{aligned} r = 0 \quad & \frac{\partial \phi}{\partial r} = 0 \quad \forall \phi \\ r = R \quad & u_z = u_r = 0 \end{aligned} \tag{42}$$

The domain is initialized with a uniform density and a parabolic velocity profile. The density is taken constant, and we apply a pressure gradient “a” along the vertical axis. Under these conditions, the exact solution $u_z(r)$ of the axisymmetric Navier-Stokes equations is given by:

$$u_z(r) = V_{max} \left(1 - \frac{r^2}{R} \right) \tag{43}$$

where r is the location along the radial direction, R is the radius of the pipe and $V_{max} = aR^2 / 4\upsilon\rho$ denotes the maximum axial velocity at the symmetric axis. The Reynolds number characterizing the Poiseuille flow is defined by:

$$Re = \frac{2V_{max}R}{\upsilon} \tag{44}$$

Five discretization grids are considered 5×5, 10×10, 20×20, 40×40 and 80×80. The flow is generated by applying an axial force $a = 4\upsilon\rho V_{max} / R^2$. The axial speed simulated along the radial direction is compared with the analytical solution, see Fig. 2. Even for

less dense meshes, the numerical solution is always very close to the analytical solution. A convergence criterion is adopted to decide when the LBM code has converged "sufficiently", which means that subsequent iterations do not give a significant increase in precision.

We can define the deviation between the numerical and analytical velocities along the z direction using the E_2 norm:

$$E_2(u) = \sqrt{\frac{\sum_{ij}\left(u_z^{numerical} - u_z^{exact}\right)^2}{\sum_{ij}\left(u_z^{exact}\right)^2}} \tag{45}$$

The steady state is obtained when the following criterion is met:

$$\frac{\|u(t) - u(t - 100\delta t)\|}{\|u(t)\|} < 10^{-7} \tag{46}$$

The error decreases as the mesh becomes thinner. We plotted the variation of the error as a function of the spatial step, and we compared it with the results of Wang et al. [27]. This evolution, presented in Fig. 3, shows that the spatial precision is of order 2.

On the other hand, the effect of the relaxation time is studied for $0.6 \leq \tau_f \leq 1.5$. The numerical solution is always very close to the analytical one; see Fig. 4, which shows the ability of our code to simulate laminar flows in typical configurations and the formulation of the LBM method introduced in this code as well as the processing of the associated boundary conditions is accurate. This Benchmark test case informs us about the quality of our code in the laminar and steady state flows case, with low Reynolds number.

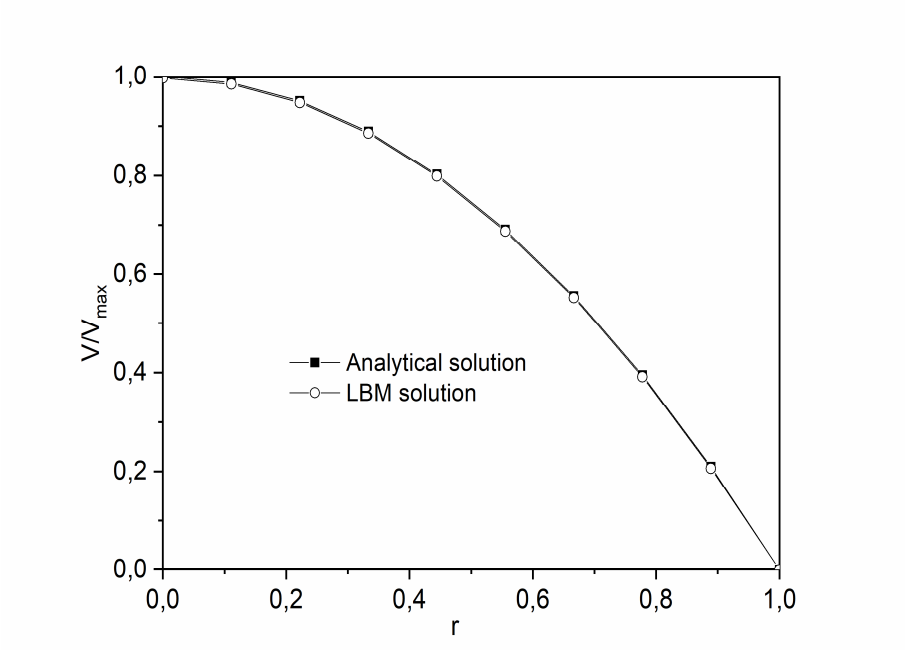

Fig. 2. Velocity profile for Re = 40, τ = 0.9 and a grid size of 10×10.

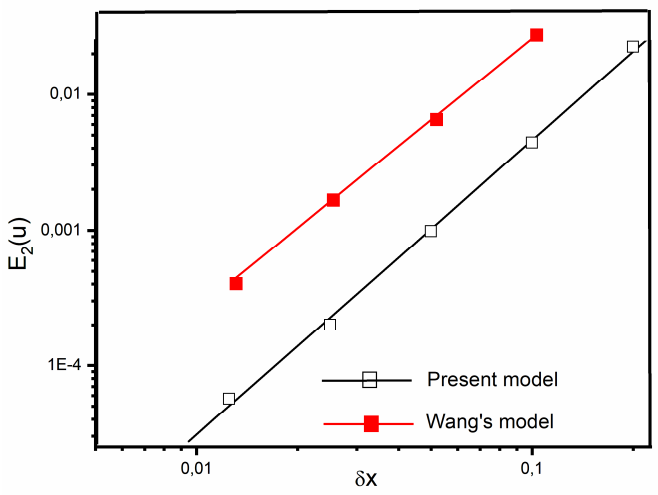

Fig. 3. Relative error of velocity as a function of spatial step for τ = 0.8.

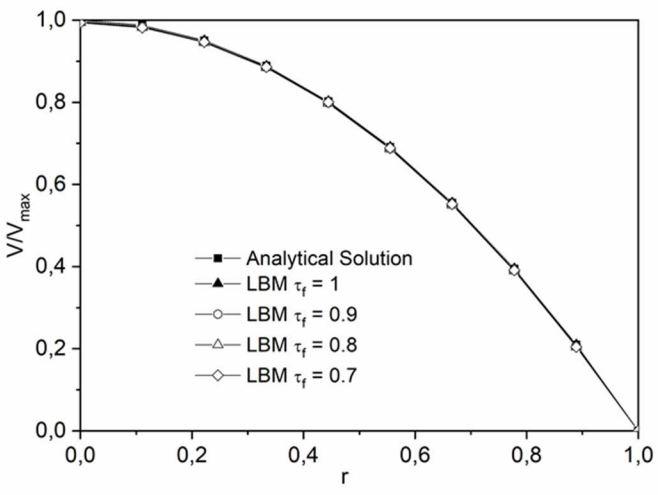

Fig. 4. Effect of dimensionless relaxation time on the velocity profile.

- Womersley unsteady flow

In this section, we have opted for investigating the accuracy of our code in unsteady state by implementing the fluid benchmark with variable control force. Indeed, the constant force in the Hagen-Poiseuille flow gives a stationary solution. If we consider a time-varying force in the form a = Acos(ωt), the axial velocity varies periodically. The analytical solution of the problem is given by:

$$u_z(r,t) = \text{Real}\left[\frac{A}{j\omega}\left(1-\frac{J_0\left(\frac{r\varphi}{R}\right)}{J_0(\varphi)}\right)e^{j\omega t}\right] \tag{47}$$

where 'Real' refers the real part of the complex variable, j is the imaginary unit, $\varphi = \alpha(j-1)/\sqrt{2}$. $\alpha = R\sqrt{\omega/\upsilon}$ is Womersley number and J_0 denotes Bessel's function of order 0 of the first type.

In the present simulation, we consider a flow characterized by a Reynolds number Re = 1200 and a Womersley number of α=8. The Reynolds number is defined here by Re = $(2RU_0)/\upsilon$ and $U_0 = (AR^2)/4\upsilon$. The relaxation parameter is fixed at τ_f = 0.8. A uniform grid of 21 × 21 is adopted in calculations. The initial conditions for the velocity are taken such that the velocity is equal to zero everywhere in the domain. The numerical results are extracted after 10 periods of calculation with the period given by: $T_p = 2\pi/\omega$. Since the problem is physically unsteady, the solution makes it possible to validate the ability of the method to describe the temporal behavior of the problems linked to the flow of fluids. Four typical times are considered for comparison with the analytical solution: $t = T_p/4, T_p/2, 3T_p/4$ and T_p. Figure 5 presents the numerical solution compared to the analytical one. As we can see, the numerical results are in good agreement with the analytical solution.

- Natural convection between two coaxial cylinders

The next validation case involves natural convection between two coaxial vertical cylinders. The problem is presented in Fig. 6. The flow is controlled by Prandtl number Pr = υ/α and Rayleigh number: $\text{Ra} = g\beta(T_i - T_o)(R_o - R_i)^2/\upsilon\alpha$ where β is the coefficient of thermal expansion and g is the gravitational acceleration. T_i and T_o are the constant temperatures imposed on the inner and outer cylinders respectively, with $T_i \geq T_o$. The horizontal walls are adiabatic. Both the radius ratio R_o/R_i and the aspect rario $L/(R_o - R_i)$ are fixed at 2. The gravitational force is given by $F_g = g\beta(T - T_{ref})$ where the reference temperature is equal to the average temperature $T_{ref} = (T_i + T_o)/2$. No-slip boundary condition is applied for boundary velocities.

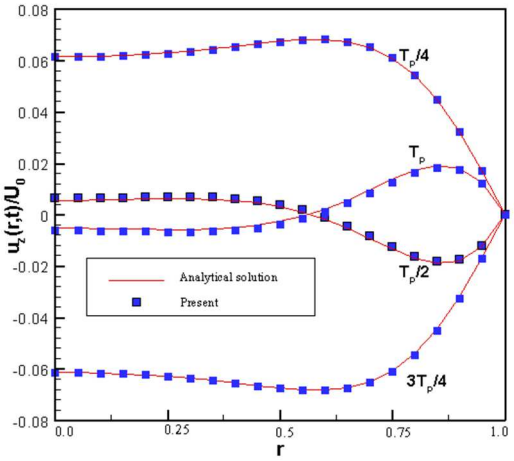

Fig. 5. Velocity of Womersley flow for Re = 1200, τ_f = 0.8 and α = 8.

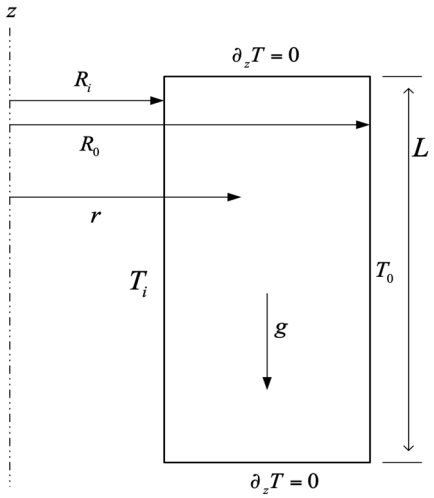

Fig. 6. Simplified 2D scheme of two coaxial vertical differentially heated cylinders.

Table 1. Comparison of the average Nusselt number with previous works.

Ra number	Kumar and Kalam [28]	Venkatachalappa et al. [29]	Chen et al. [30]	Present work
10^4	3.037	3.163	3.216	3.204
10^5	5.760	5.882	5.782	5.734

Numerical simulations are performed for Rayleigh numbers Ra = 10^4 and Ra = 10^5. The mesh considered for this test case is 100×200. Figure 7 shows the streamlines and the isothermal lines. The isothermal lines show that as the Rayleigh number increases, the thermal boundary layer becomes thinner, and the velocity becomes important near the walls. These results are in good agreement with the results of reference [29-31]. Quantitatively, we calculated the Nusselt number on the inner wall defined by:

$$Nu = \frac{r_i}{T_i - T_0} \int_0^L \left. \frac{\partial T}{\partial r} \right|_i dz \tag{48}$$

This average Nusselt number is compared to the reference results in Table 1. We note a good agreement with the results of references.

- Natural convection with solid/liquid phase change

In this section, we will verify the accuracy and reliability of our model by examining thermal convection coupled with the solid / liquid phase change. Indeed, in the previous cases, the studies involved a single phase with fixed or periodic boundaries; while in this case, the flow occurs in a domain with a moving boundary. The adopted approach to handle this boundary is the enthalpy method, which enables the determination of the molten fraction at each node without requiring precise knowledge of the solid/liquid interface position. Consequently, within the solid zone, the fluid flow is non-existent, and only thermal phenomena are considered. In the liquid phase, where the liquid fraction equals 1, the flow is influenced by gravitational forces and is coupled with thermal phenomena. In the intermediate zone, the liquid fraction lies between 0 and 1. The considered configuration is a cylindrical cavity with an aspect ratio of 2. The horizontal walls are considered adiabatic, while the vertical walls are assumed to be isothermal, maintained at hot and cold temperatures T_H and T_C, respectively, as shown in Fig. 8.

Figure 9(a) illustrates the flow structure at various Fourier numbers, specifically Fo = 1, Fo = 5, and Fo = 10. During the initial melting phase, thermal diffusion plays a dominant role in the thermal transfer mechanism. The solid/liquid interface advances parallel to the vertical wall. In the case of Fo = 1, small vortices are formed. However, these vortices are of low intensity and do not exert a significant impact on the deformation or advancement rate of the solid/liquid interface. Thermal diffusion remains the primary mechanism governing the process. Over time, the flow is characterized by cells that merge with each other, which justifies the periodic behavior of the maximum velocity in Fig. 11.

As time progresses, the fluid zone expands, and the cells within it intensify, leading to a marked deformation of the solid/liquid interface, particularly on the upper side of the cavity. Figures 9 and 10 show a good agreement of our results with the work of Li et al. [31], which confirms the ability of our code to simulate accurately similar solid / liquid phase change problems. In Fig. 11, we present the evolutions of the Nusselt number and maximum velocity as a function of time. The Nusselt number exhibiting heat transfer from the hot wall side, as well as the maximum velocity, varies periodically with time and this is due to vortex oscillations with increasing Fourier number.

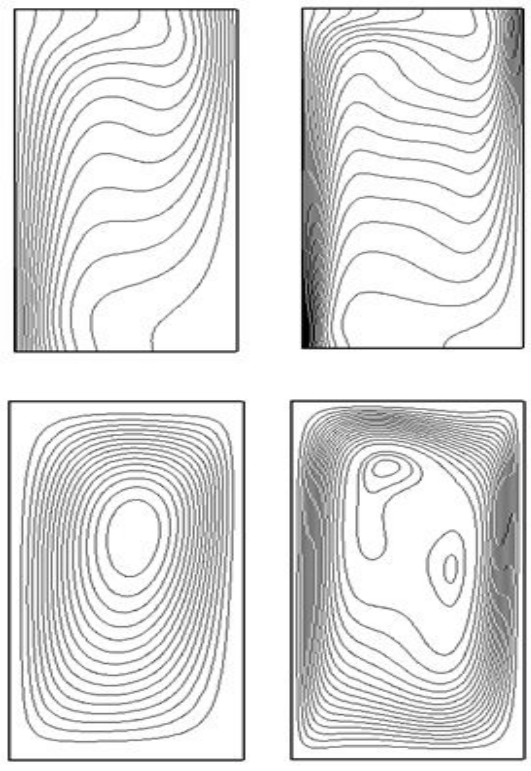

Ra = 10^4 Ra = 10^5

Fig. 7. Isotherms (top) and streamlines (down) for two Rayleigh numbers at Pr = 0.7.

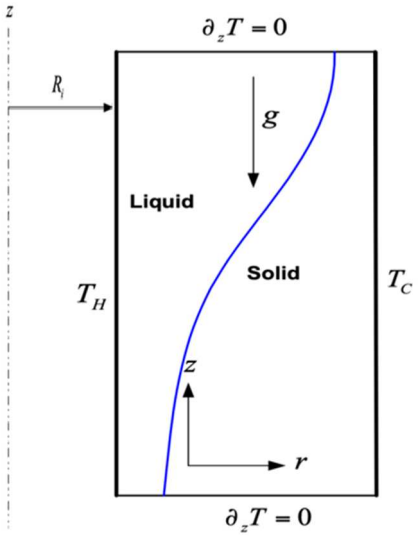

Fig. 8. Configuration of a solid/liquid phase change problem.

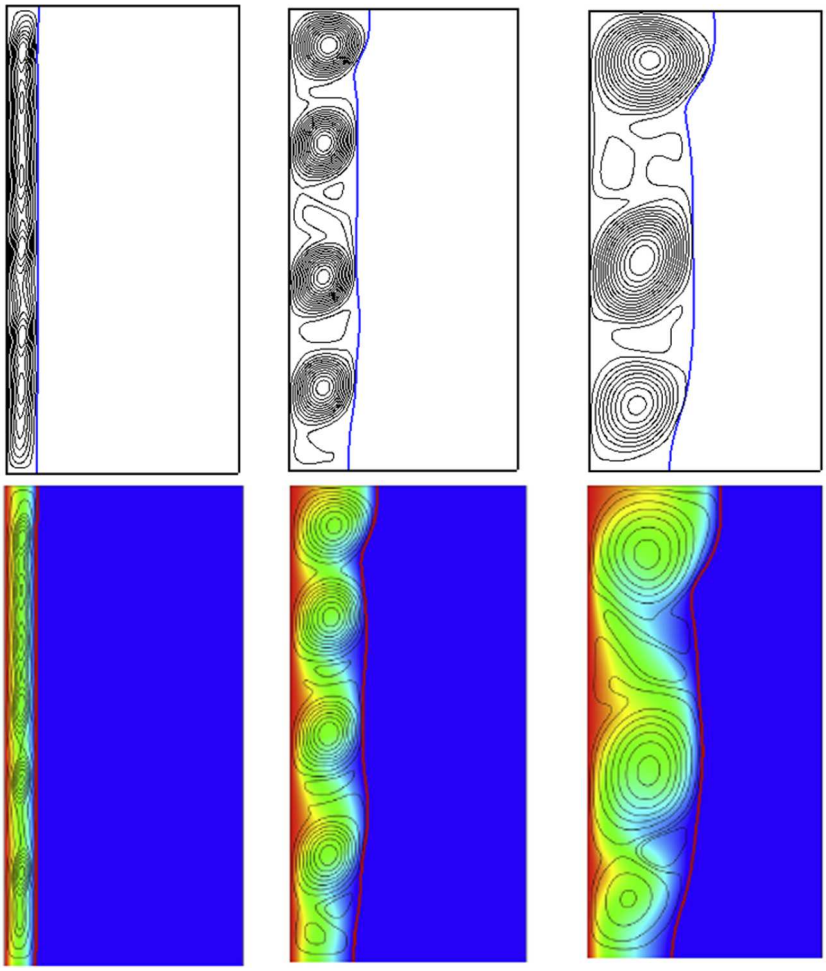

Fig. 9. Solid/liquid interfaces obtained by our code (top) and Li et al. [31] (down) for different Fourier numbers.

3. Results and Discussion

The results of this study are presented in the form of isotherms, streamlines, melt front, liquid fraction, temperature, Nusselt number, and geometric characteristics of the inserted metal fins. The aim of this study is to conduct a numerical investigation of the latent heat thermal energy storage system (LHTES) by solid-liquid phase change. Metal fins are inserted within the domain occupied by the PCM to improve the heat transfer. The numerical simulations were made using a heat transfer fluid with a Prandtl number of Pr = 2.2. The PCM considered in this study is characterized by a Prandtl number of Pr = 12.5 and the fins have a thermal conductivity 600 times higher than that of the PCM. The remaining control parameters are the aspect ratio of the cavity

taken equal to 1, the Reynolds number Re = 50, the inlet temperature of the heat transfer fluid T_{in} = 1 and the number of fins mounted to improve the storage process which will vary according to each studied case. These parameters are considered for a qualitative analysis of the problem. To determine the appropriate grid resolution for the current study, a grid independence test is conducted using three different grid configurations 60×60, 80×80 and 160×160. Figure 12 shows the effect of grid size on the variation of Nusselt number with liquid fraction for different grids. It can be deduced from this figure that the mesh 80×80 gives satisfactory results and can be adopted for the numerical simulation of our problem.

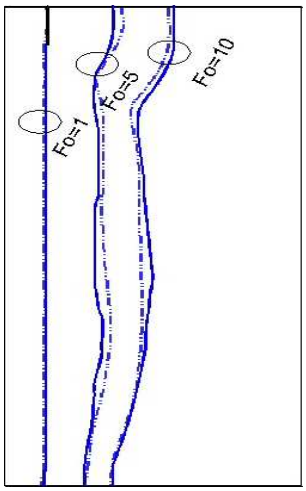

Fig. 10. Comparison between our results (dashed) and those of Li et al. [31] (line) in term of solid/liquid interface for different Fourier numbers.

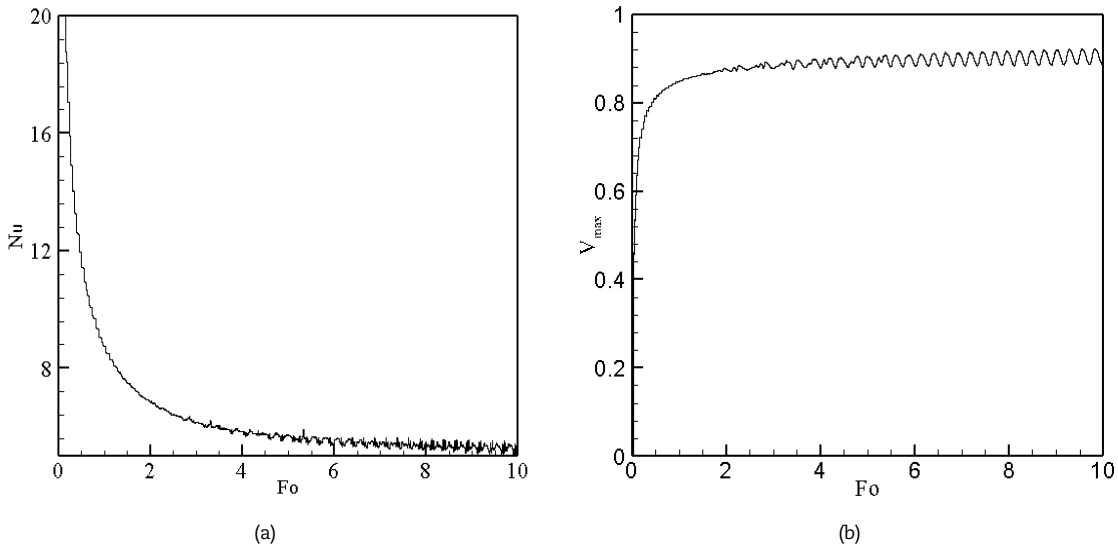

Fig. 11. Evolution of (a) Nusselt number and (b) maximal velocity as a function of Fourier number.

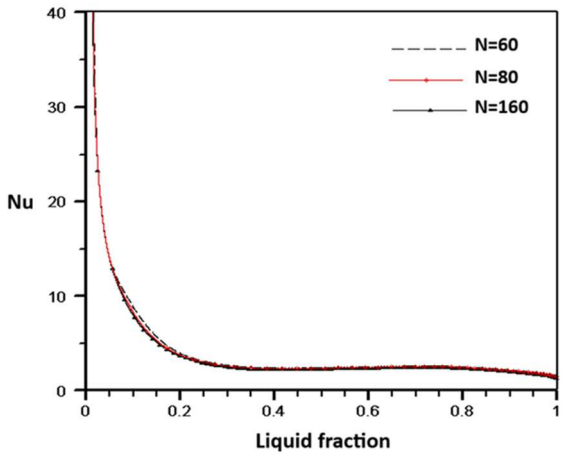

Fig. 12. Variation of the Nusselt number with liquid fraction for different grid sizes.

3.1. General trends of heat transfer: Analysis of isotherms and streamlines

In order to understand the mechanisms of heat transfer involved in the phase change process of the PCM, isotherms and streamlines are drawn in Fig. 13 for different times and two values of Rayleigh number Ra = 0 and Ra = 2×10^5.

Firstly, for Ra = 0, it is clear that isotherms evolution remains practically parallel to the wall during the melting process. The heat transfer mechanism is primarily governed by pure thermal conduction, predominantly in the radial direction. Initially, the melting front advances rapidly, leading to a significant heat flux transmission. As the interface continues to progress, the thermal resistance between the hot zone on the Heat Transfer Fluid (HTF) side and the cold zone becomes increasingly significant.

For Ra = 2.5×10^5 and at the beginning of the melting process, isotherms are almost parallel to the wall because of the dominance of thermal conduction and we have a small amount of melted PCM, which is not sufficient to impact the structure of the isotherms. When the melting front progresses and by increasing the amount of liquid PCM, we notice the appearance of flow cells in the fluid zone and there is a clear distortion of the isotherms. In addition, the hot liquid PCM rises to the upper side because of a decrease in its density and the cold liquid PCM falls to the bottom side. This explains the curvature of the melting front on the upper side. On the other hand, the flow cell enhances the heat transfer to the solid zone, resulting in the accelerated melting process in the upper part. As for the evolution of the streamlines, the liquid PCM flow is single-cell clockwise. The maximum flow intensity is located at the center of the vortex.

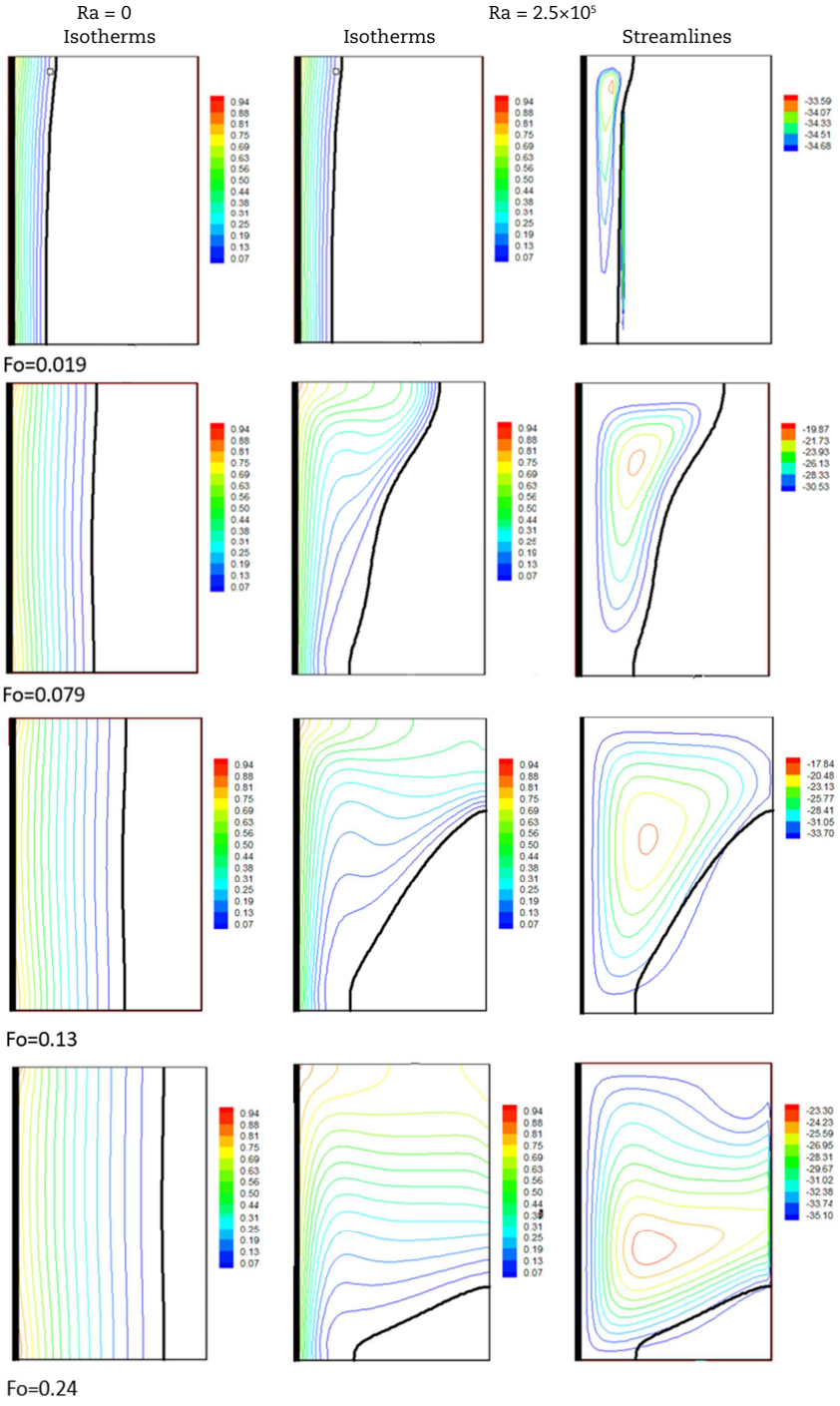

Fig. 13. Evolution of isotherms and streamlines as a function of Fourier number for Ra = 0 and Ra = 2.5×10^5.

3.2. Effect of natural convection

Figure 14 shows the evolution of the PCM liquid fraction for two cases: Ra = 0 (without natural convection) and Ra = 2.5× 10^5 (with natural convection). The melting process begins with the formation of a thin liquid film around the Heat Transfer Fluid (HTF) tube. This liquid film progressively expands until reaching the time corresponding to the Fourier number Fo = 0.07. Throughout this phase, the evolution of the liquid fraction remains consistent in both cases, with and without natural convection, as evidenced by the convergence of the two curves within the time interval [0 - 0.07]. This behavior can be attributed to the thin fluid zone dominated by the conductive regime, leading to a maximal thermal resistance. As a result, there is a rapid and linear increase in the liquid fraction during this initial phase. However, as the fluid zone thickness expands, the effect of natural convection becomes more pronounced. This intensifies the heat transfer to the PCM, resulting in a larger liquid fraction. The presence of natural convection accelerates the PCM melting process significantly. Consequently, the contribution of convection to heat transfer within the PCM reduces the charging time (PCM melting) by approximately 25% compared to the case without convection.

The effect of natural convection can also be illustrated by the behavior of the outlet temperature of the channel in Fig. 15. It varies between 0.6 and 0.7 for the major range of Fourier number Fo, while it remains around 0.9 in the case without natural convection. Indeed, for Ra = 2.5×10^5, the heat transfer of the fluid towards the heat exchanger becomes more important, resulting in a strong thermal gradient between the inlet and the outlet of the channel. The outlet temperature, as represented in Fig. 15, shows a trend of the variation either the same at the beginning of the melting process for the cases without and with natural convection. Subsequently, it is noticed that the outlet temperature in the case without natural convection increases rapidly compared to the case where the effects of natural convection are taken into account. This indicates that taking natural convection into consideration leads to an increase in the temperature difference between the inlet and the outlet HTF temperature. This behavior is likely to improve the heat transfer. This significant heat transfer is also evident from the evolution of the Nusselt number, as shown in Fig. 16. Initially, in both cases, the heat transfer is primarily conductive, and the Nusselt number exhibits a similar trend. However, as the fluid zone reaches nearly 25% of the liquid PCM volume, convection emerges, resulting in a considerable improvement in heat transfer.

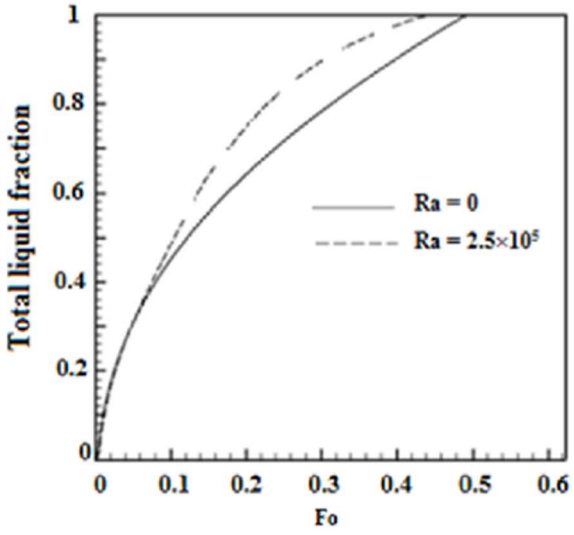

Fig. 14. Total liquid fraction evolution as a function of Fourier number for Ra = 0 (solid) and Ra = 2.5× 10^5 (dashed).

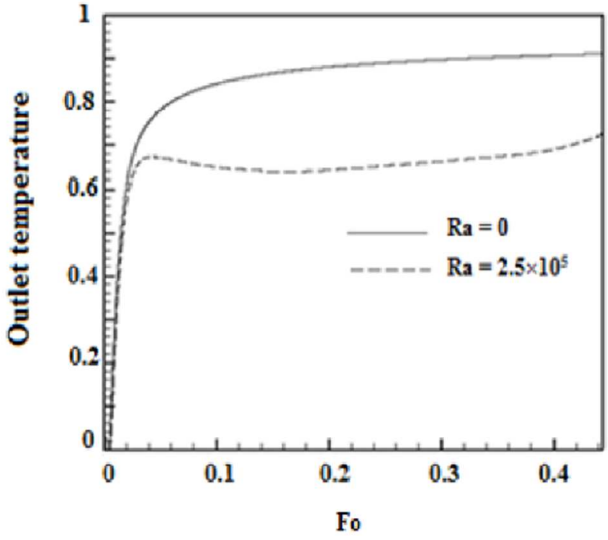

Fig. 15. Dimensionless outlet temperature of the channel evolution as a function of Fourier number for Ra = 0 and Ra = 2.5× 10^5.

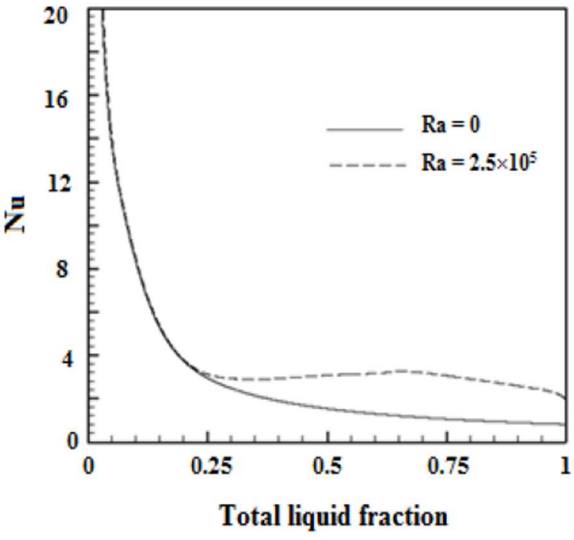

Fig. 16. Evolution of the average Nusselt number as a function of the total liquid fraction for Ra = 0 and Ra = 2.5× 10^5.

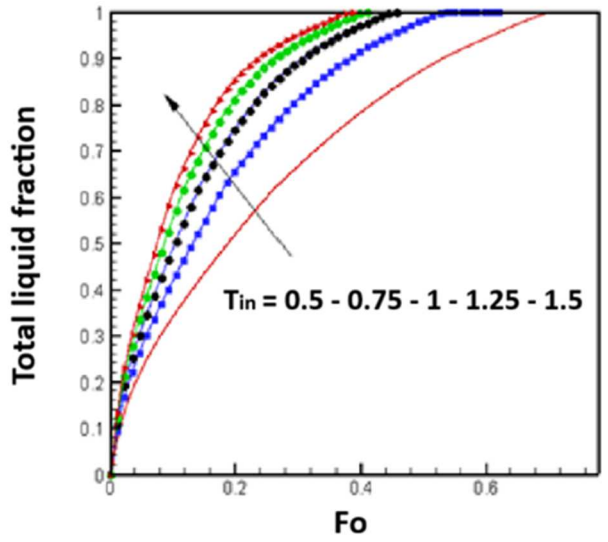

Fig. 17. Liquid fraction evolution as a function of Fourier number for different inlet temperatures.

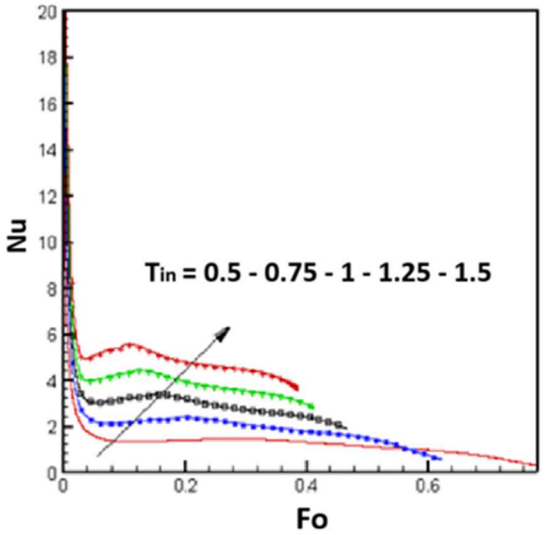

Fig. 18. Average Nusselt number evolution as a function of Fourier number for different outlet temperatures.

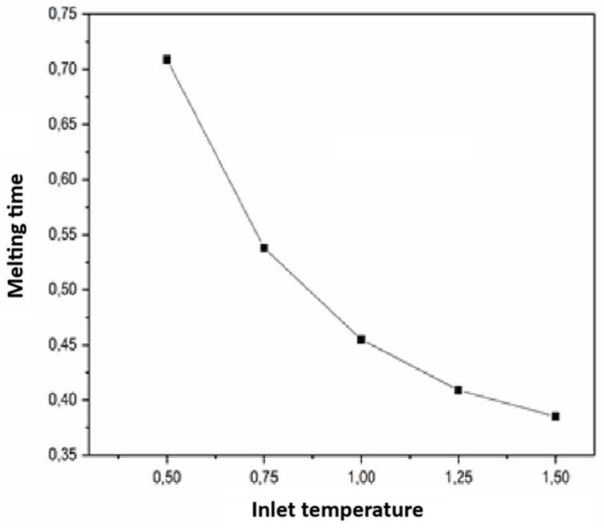

Fig. 19. Variation of the total melting time with the inlet temperature.

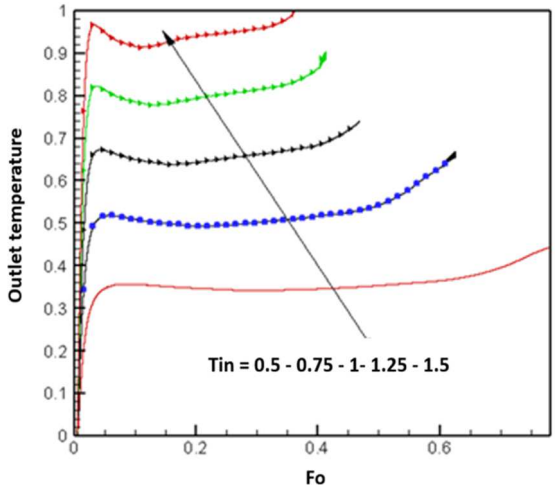

Fig. 20. Outlet temperature evolution as a function of Fourier number for different values of the inlet temperature.

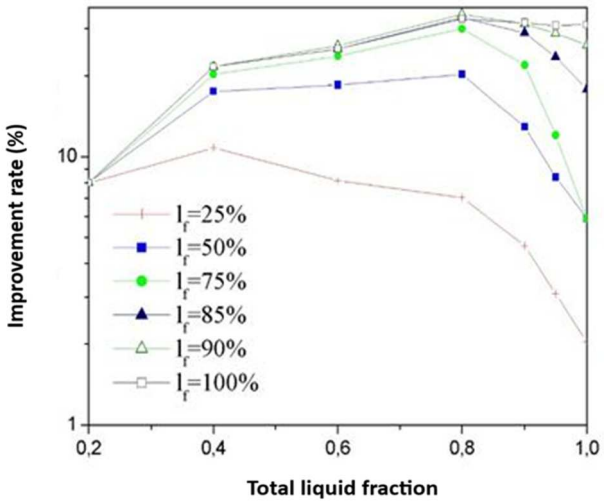

Fig. 21. Effect of fin length on the PCM melting time for Ra = 2.5× 10^5.

3.3. Effect of inlet temperature

The impact of the inlet temperature on the evolution of the liquid fraction and the total melting time is illustrated in Fig. 17 and Fig. 18, respectively. Evidently, as the HTF inlet temperature increases, the total melting time of PCM decreases. This signifies a higher rate of liquid fraction evolution over time. Comparatively, the PCM in the unit with a higher injection temperature always melts faster than that in the unit with a lower injection temperature. The rise in inlet temperature enables a greater amount of thermal energy to be injected into the channel by the heat transfer fluid. This evolution of the total melting time is also explained by the evolution of heat transfer rate. Indeed, as shown in Fig. 18, increasing the HTF inlet temperature results in a higher average Nusselt number and consequently reduces the time required for total melting. This indicates that raising the HTF inlet temperature enhances heat transfer within the PCM, leading to faster energy storage within the material.

Based on the results obtained in Fig. 19, it can be shown that the melting time evolves with the inlet temperature according to the following expression: $t_m = 0.36 + 1.31e^{(-T_{in}/0.37)}$.

The effect of the HTF inlet temperature on the temporal evolution of the outlet temperature is also revealed in Fig. 20. Despite different HTF inlet temperature values, the evolution of the outlet temperature exhibits similar patterns. Increasing the HTF inlet temperature results in a rise in the outlet temperature of the HTF, accompanied by a reduction in the total time required for PCM melting. The disparity between the inlet and outlet temperatures serves as an indicator of the heat exchange rate between the channel and the base PCM.

3.4. Effect of fin insertion

Since PCMs suffer from their low effective thermal conductivity, several techniques are possible for improving the effective thermal conductivity. In our present work, we opt for the insertion of metallic fins within the domain occupied by PCMs. To reveal the effect of the insertion of metallic fins on the thermal and hydrodynamic behavior of the PCM, a fin is mounted in the center of the enclosure.

The impact of fin length on the total PCM melting time is illustrated in Fig. 21. Fin sizes less than 25% show a modest enhancement for low liquid fractions, reaching up to 10%. This improvement rate starts to decrease while approaching the mass of the liquid PCM until it becomes very small. On the other hand, for sizes exceeding 50% of the length of the liquid zone, a notable improvement in melting time is observed. This gain surpasses 30% for a liquid fraction of 90%. The curve relating to the

rate of improvement of the charging time of 85% coincides practically with those relating to 90% and 100%. Based on the results obtained, a fin size of 85% of the length of the liquid zone can be considered as the optimum size giving rise to a significant gain in melting time.

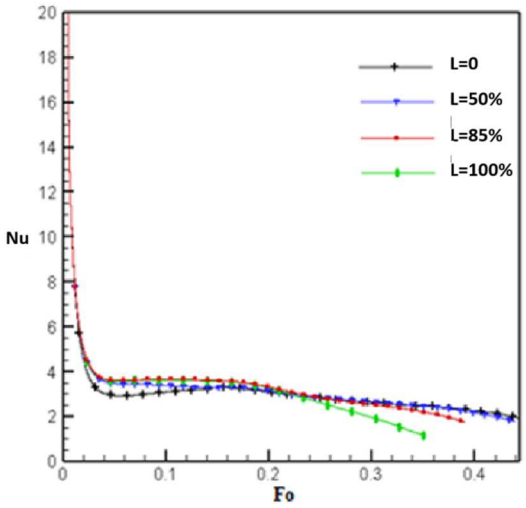

Fig. 22. Average Nusselt number evolution as a function of Fourier number for different fin lengths.

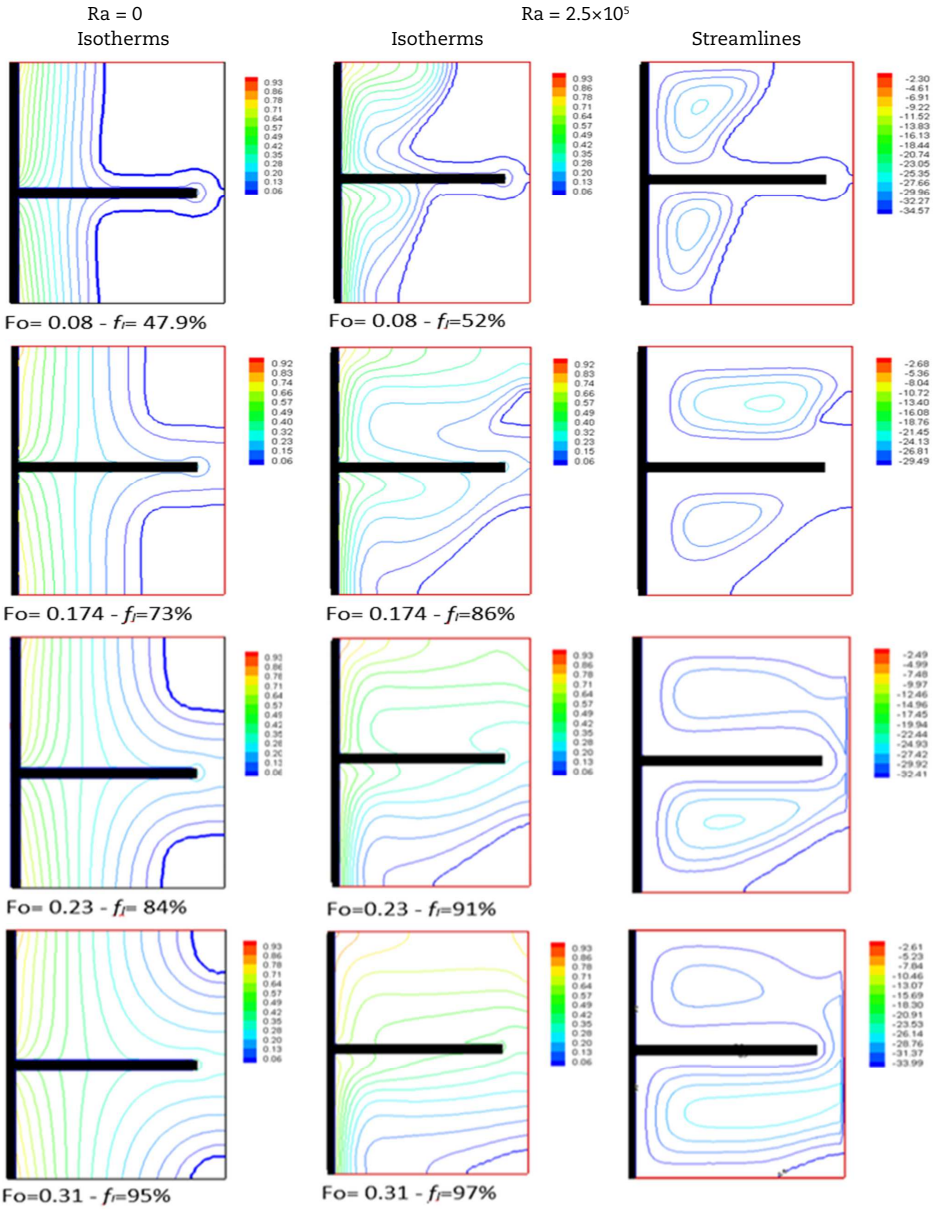

Fig. 23. Evolution of isotherms and streamlines as a function of Fourier number for Ra = 0 and Ra = 2.5×10⁵ with L = 0.85.

Additionally, the performance of heat transfer in LHTES can also be evaluated by monitoring the temporal evolution of the average Nusselt number. This evolution is shown in Fig. 22. It is clear that the heat flux through the vertical walls decreases as the melting time progresses. The evolution of the average Nusselt number is split into three stages. At the beginning of the melting process, the average Nusselt number shows a rapid and linear decrease. This decrease is due to the fact that the heat transfer is initially governed by pure heat conduction. The enlargement of the liquid PCM zone develops the appearance of natural convection during the phase change of the PCM and the evolution of the average Nusselt number is characterized by a plateau of almost constant value. In a third stage, the heat transfer performance starts to decrease again by decreasing the average Nusselt number. In fact, this is the new appearance of heat conduction. This is the mutual existence of natural convection and thermal conduction. For fin sizes greater than 50% (85% and 100%), the rate of decrease in thermal performance is maximal.

The addition of fins to the LHTES system reduces the melting time. Indeed, the presence of fins will contribute to increase the heat transfer surface. In order to describe the contribution of natural convection to the phase change process in the presence of fins, we consider the case of one fin mounted and we present in Fig. 23, isotherms and streamlines for Ra = 0 and Ra = 2.5×10^5 and for times corresponding to the Fourier numbers Fo of 0.08 – 0.174 – 0.23 – 0.31.

For Ra = 0, isotherms remain almost parallel to the hot wall with a weak deformation around the fin; this is due to the effect of the high values of the thermal conductivity of the fins leading to a rapid transfer of heat towards the PCM.

For Ra = 2.5×10^5, as discussed in the case without fins, the beginning of the melting process is governed by the thermal conduction mechanism. This conduction transfer process is reinforced by the fin which causes a deformation of the isothermal lines in the zones close to it. When the time advances, at Fo = 0.08, the fluid zone becomes more important and the confined spaces on the sides of the fins are practically melted. The fluid in the confined areas heats up along the hot vertical wall and then deflects towards the solid PCM after reaching the top surface. This hot flow hits the solid-liquid interface and cools along the interface. This intensifies the convective motions produced by the thermal gradient between the solid-liquid interface and the wall on the HTF side giving rise to two clockwise flow cells in the two confined areas.

For Fo = 0.174, the fluid zone becomes larger and occupies more than 86% of the cavity. Isotherms are practically stratified in the upper confined spaces. The settlement cells remain attached to the solid-liquid front. For Fo = 0.23, the flow cell in the upper zone contributes to the heating of the fluid and increases the energy accumulation by sensible heat in the upper zone. However, since the flow cells remove heat from the HTF fluid to the cooler fluid zones, much of the heat is transferred to the upper fluid zone resulting in temperature stratification. The melting is mainly done by conduction which justifies the slowing down of the melting process during this phase. To analyze this phenomenon, we have plotted the temporal evolution of the sensible heat with and without fins. In the case without fins in Fig. 24, the sensible heat storage in the fluid can be divided into two phases. During the first phase going from Fo = 0 to Fo = 0.14, the interface always connects the upper wall to the lower wall and the exchange surface of the PCM solid zone with the fluid zone is important leading to a large latent heat transfer. At the time Fo = 0.14 corresponding to a liquid fraction of 70%, the upper end of the interface coincides with the right corner of the cavity and the exchange surface will start to decrease from this moment. The heat extracted from the HTF is then more and more stored by sensible heat in the upper fluid zone which justifies the inflection point at this moment and the increase of the sensible heat storage rate. In the case with fins (for example here for two fins), this inflection point still persists but occurs for increasingly higher liquid fractions, Fig. 25. The inflection point corresponding to the change of rapidity of the sensitive energy storage occurs at the time Fo = 0.18 for a total liquid fraction of 92%.

For the case of two fins, Fig. 26 shows isotherms and streamlines for Ra = 0 and Ra = 2.5×10^5 at different instants corresponding to the Fourier numbers Fo of 0.03 – 0.125 – 0.176 – 0.26. For Ra = 0, isotherms are parallel to the left vertical wall at the beginning. Then just after, they undergo a deformation due to the presence of the fins which accelerates the heat transfer to the PCM. These deformations become more marked with time and in an almost symmetrical way.

For Ra = 2.5×10^5, at the beginning of the melting, the transfer is dominated by thermal conduction with a deformation close to the fins. With time, the fluid zone becomes larger and gives rise to the development of convective cells in the three microcavities bounded by the fins. The upper cell is more intense which affects considerably the isothermal lines in this region with a faster progression of the solid/liquid interface.

At Fo = 0.176, the melting rate of the PCM changes trend and becomes very slow. This is due to the fact that from this moment, a large part of the thermal energy is stored by sensible heat in the upper fluid zones which slows down the heat transfer to the solid zone of the PCM.

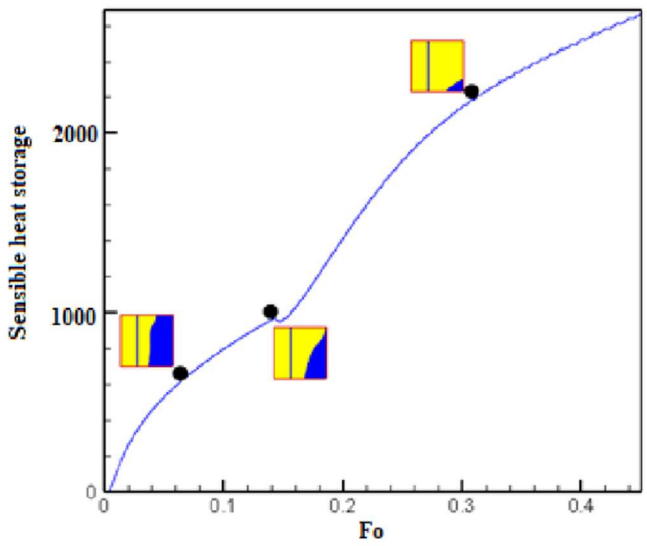

Fig. 24. Sensible heat storage evolution as a function of Fourier number and the solid-liquid interface without fin.

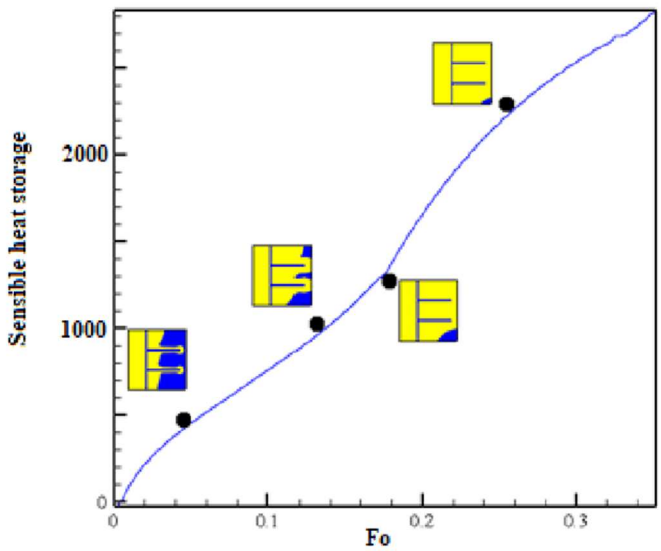

Fig. 25. Sensible heat storage evolution as a function of Fourier number and the solid-liquid interface with two fins.

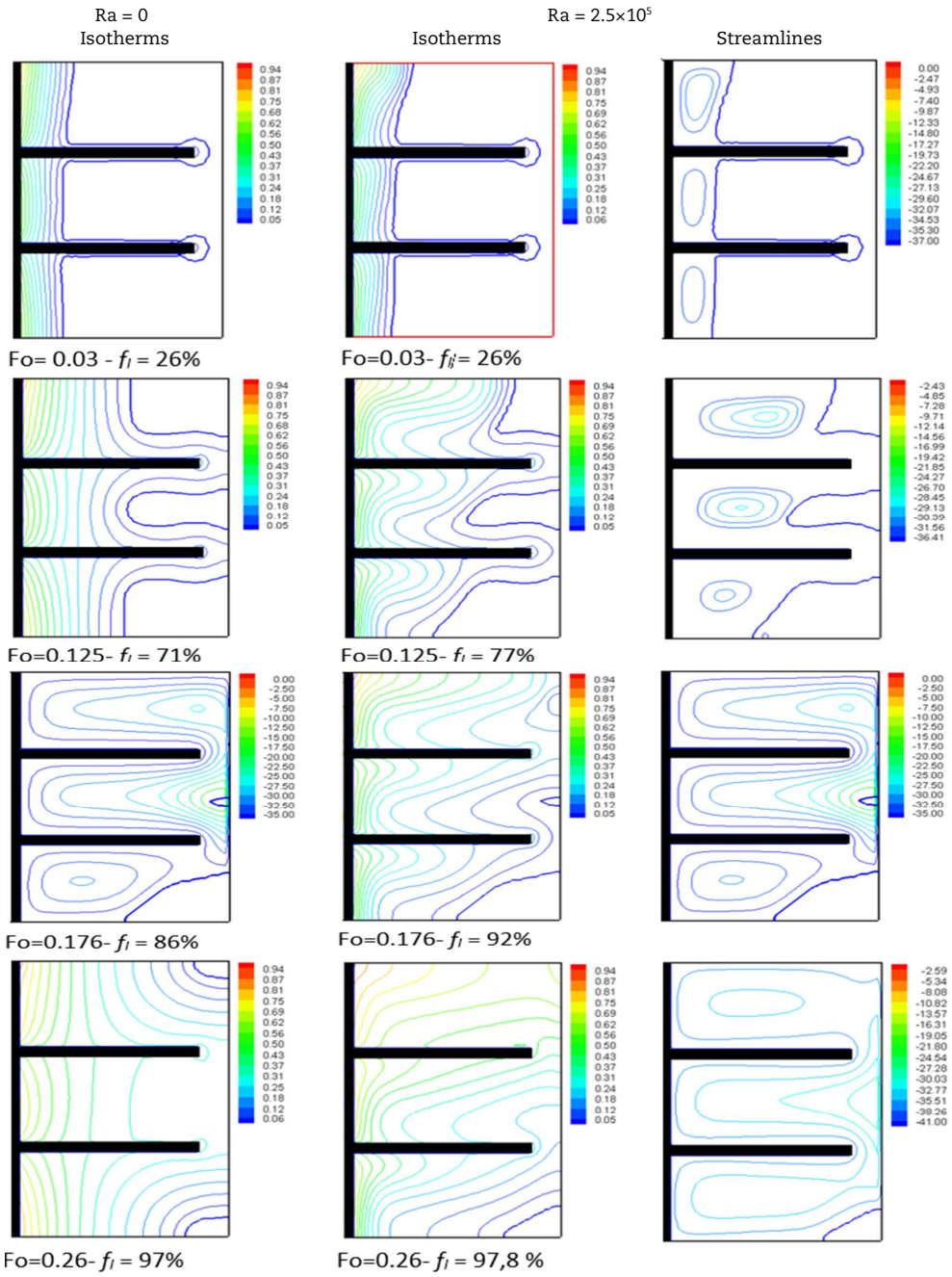

Fig. 26. Isotherms and streamlines with two fins of L = 0.85.

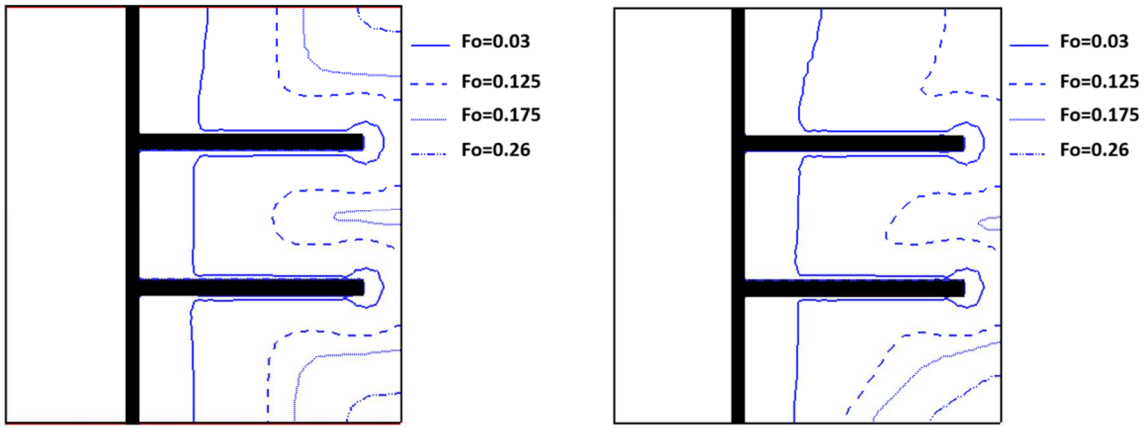

Fig. 27. Solid-liquid interface for different Fourier numbers with Ra = 0 (left) and Ra = 2.5×10^5 (right).

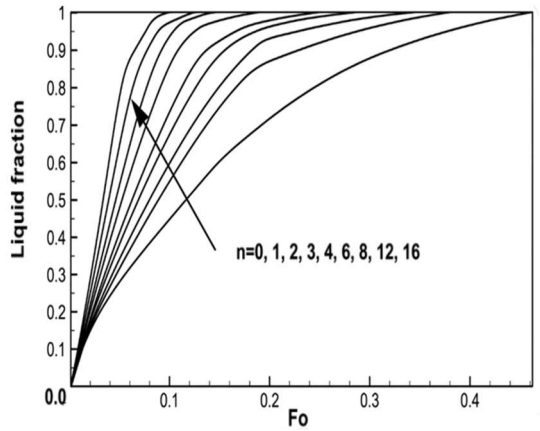

Fig. 28. Effect of the number of fins on the total liquid fraction evolution with Ra = 2.5×10^5.

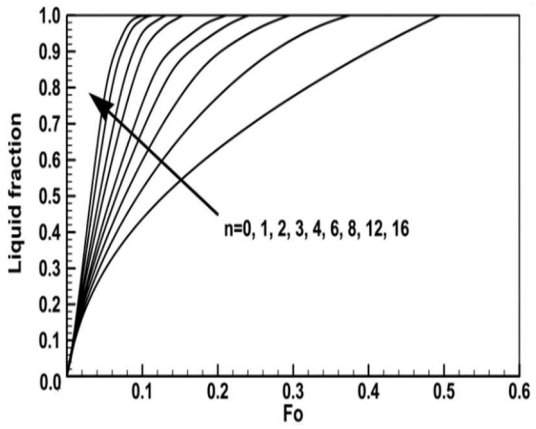

Fig. 29. Effect of the number of fins on the total liquid fraction evolution with Ra = 0.

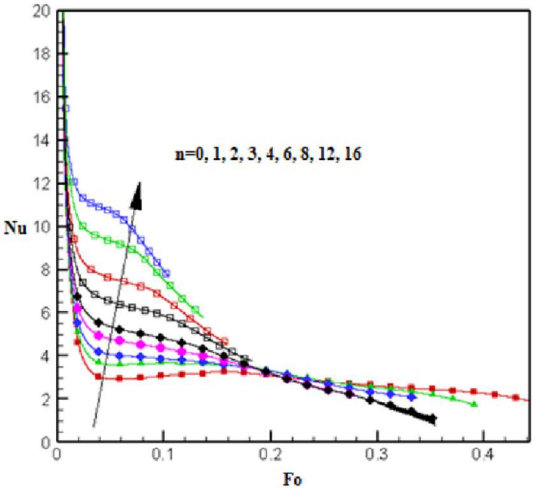

Fig. 30. Effect of the number of fins on the average Nusselt number with Ra = 2.5×10^5.

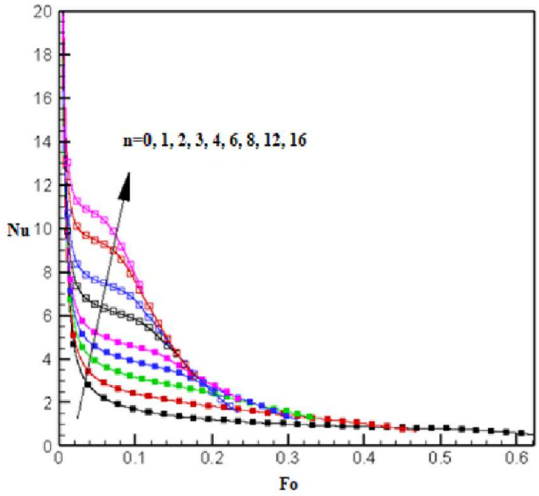

Fig. 31. Effect of the number of fins on the average Nusselt number with Ra = 0.

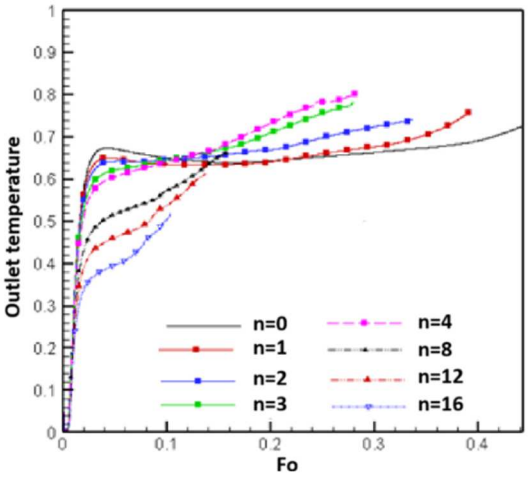

Fig. 32. Variation of the outlet temperature for different numbers of fins with Ra = 2.5×10^5.

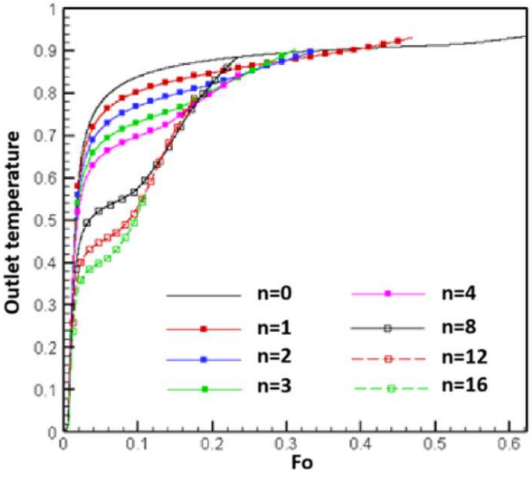

Fig. 33. Variation of the outlet temperature for different number of fins with Ra = 0.

Figure 27 shows the evolution of the melting front in the two cases Ra = 0 and Ra = 2.5×10^5 for different times: Fo = 0.03, 0.125, 0.175 and 0.26. During the initial phase of melting, a thin layer of molten PCM forms parallel to the surface of the tube and fins, primarily driven by the dominant heat conduction mechanism. In the case of Ra = 0, the interface evolves symmetrically. However, for Ra = 2.5×10^5, the thickness of the molten PCM layer at the top is greater than that at the bottom due to the gradual decrease in the HTF inlet temperature along the flow direction. As time progresses, it becomes evident that the PCM adjacent to the tube and fin surface completely melts, as the temperature of the liquid PCM at the top is higher than that at the bottom. The shape of the solid-liquid interface changes curvature due to the effect of natural convection. At the time Fo = 0.175, almost 92% of the PCM is melted, most of which corresponds to the upper two zones. There remains only a small part of the lower zone which melts very slowly which justifies the inflection point for Fo = 0.175. After this inflection point, the liquid fraction increases from 92% to 100% and spends a lot of time to do so.

Figures 28 and 29 represent the variations of liquid fraction versus time for the two cases with and without convection for different number of fins respectively. We proceeded to the finning while keeping the same mass of the PCM to have a clearer idea on the performance of the system. In both cases with and without natural convection, the higher the number of fins is, the more the melting time is reduced, see Fig. 15 and Fig. 16. For the same mass of PCM and with 16 fins, we can improve the melting time by almost 80%. This improvement is impacted by the intensity of the natural convection especially for the reduced number of fins, which gives more space to the development of natural convection. These natural convection movements lead to an accumulation of energy in the upper zones, which delays the melting of the lower parts of the PCM. The evolution of the liquid fraction can be considerably accelerated by adopting a large number of fins because the fins extend the heat transfer area and conduct the heat directly to the PCM inside.

The effect of this increase of the exchange surface with the PCM on the heat transfer is clearly seen in the behavior of the Nusselt number. The increase in the number of fins improves the heat transfer rate in both cases studied, see Fig. 30 and Fig. 31. In addition, when the Nusselt number decreases, more heat is dissipated to the outside, which justifies the increase in the outlet temperature, see Fig. 32 and Fig. 33. As a result, it can be said that increasing the number of fins in the LHTES system improves the heat transfer by increasing the average storage power and thus reducing the melting time. However, beyond a certain number of fins, the additional extension of the heat transfer area has little effect on the system performance.

As discussed in the previous sections, the complete melting time can be reduced by adding radial fins. With four fins, in the presence of natural convection, the melting time is improved by 44%. This improvement is even more important in purely conductive regime and reaches 57%. This difference is due to the fact that the convective movements cause a heat accumulation in the upper liquid zones and thus slow down the melting of the lower zone; thus, a large amount of heat would be trapped between the upper zones between fins. This justifies the difference in the improvement rates in the two cases with and without natural convection. The greater the number of fins is, the shorter the melting time is, see Fig. 29. We notice that the improvement becomes more important in the diffusive case (Ra = 0). When the number of fins is higher than 12, the convective transfer becomes negligible before the conductive one and the thermal and dynamic behavior of the system becomes similar in both cases. The melting time as a function of the number of fins can be estimated by:

$$t_m = 0.103 + 0.39e^{(-n/3.9)} \quad \text{for} \quad \text{Ra} = 0 \tag{49}$$

$$t_m = 0.119 + 0.455e^{(-n/6.186)} \quad \text{for} \quad \text{Ra} = 2.5\times10^5 \tag{50}$$

By increasing the thickness of the fin, the contact area between the fin and the heating tube expands, subsequently reducing the resistance to heat transfer. As a result, the melting rate of the phase change material increases, leading to a decrease in the overall melting time. To investigate the impact of fin thickness on the performance of the Latent Heat Thermal Energy Storage (LHTES) system, a system with three fins is considered. Figure 34 shows the variation of the total melting time with the fin thickness. The augmentation of the fin thickness favors a greater transfer of heat to the Phase Change Material (PCM). Notably, the acceleration of the melting process is particularly evident for thicknesses below 0.09. Beyond this value, the enhancement in melting time becomes limited. Moreover, the increase in thickness necessitates more metal mass, resulting in a higher aspect ratio for the same mass of PCM. Therefore, a comprehensive technical-economic study is crucial to make an informed decision regarding the appropriate fin thickness. The quantitative effect of the thickness on the melting time can be given by the expression:

$$t_m = \text{th}^{-0.417} \tag{51}$$

3.5. Charge and discharge

Natural convection occurs in the molten PCM and is controlled by the thermal gradient T_H - T_m. However, during solidification, the phase change is managed by the discharge temperature T_C - T_m. During the melting phase, natural convection plays a significant role in influencing the evolution of the liquid fraction. However, during solidification, natural convection becomes merely an initial condition for the problem and its influence diminishes significantly [32].

In this study, the discharge process is investigated after partial melting of the PCM, corresponding to initial liquid fractions of 0.5, 0.75, 0.9, and 1. Figure 35 illustrates the temporal evolution of the total liquid fraction as a function of the Fourier number (Fo) for the different initial discharge conditions. For the complete charging cycle (initial liquid fraction = 1), the PCM reaches full melting at Fo = 0.445. From this point onward, the discharge process starts, and the liquid fraction gradually decreases until complete solidification is achieved at Fo = 1. The solidification curves exhibit an approximately linear decrease over most of the discharge period, indicating a nearly constant solidification rate during this stage. Slight deviations from linearity are observed at the beginning and toward the end of the process, reflecting the transient thermal response of the PCM.

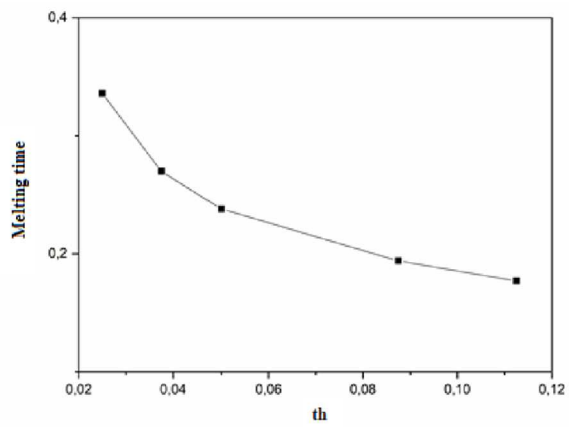

Fig. 34. Total melting time versus fin thickness with 3 fins.

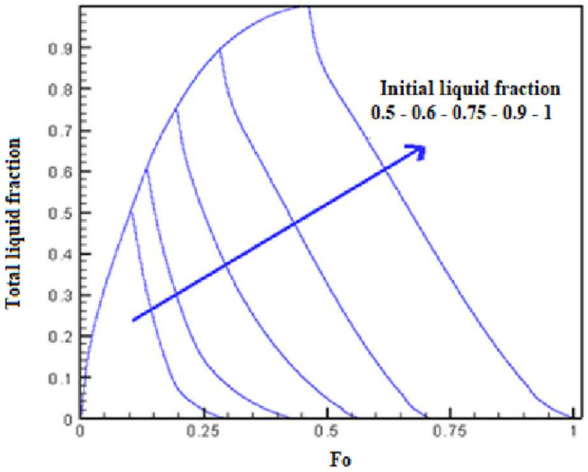

Fig. 35. Total liquid fraction evolution as a function of Fourier number with different initial conditions.

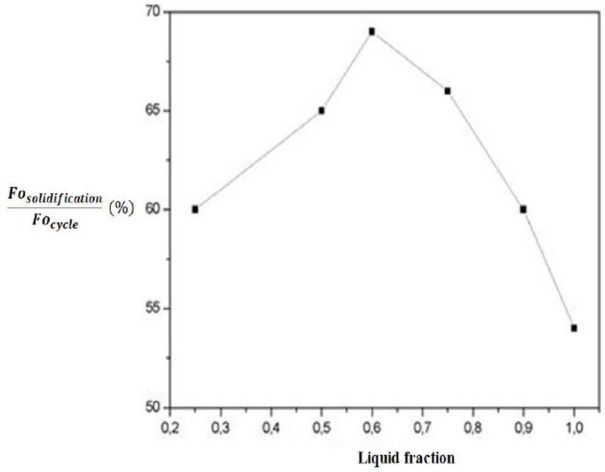

Fig. 36. Variation of the relative solidification time as a function of the initial liquid fraction.

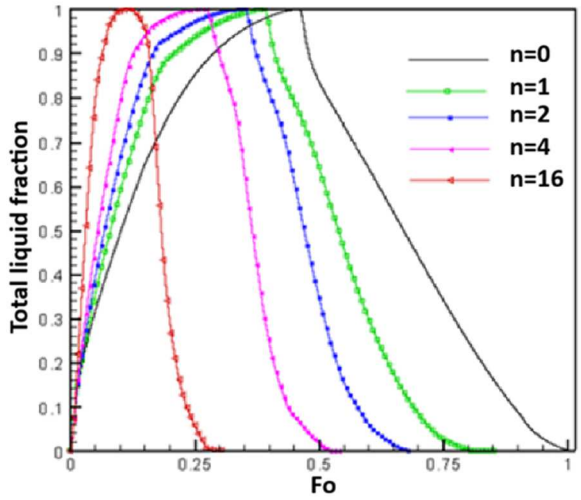

Fig. 37. Total liquid fraction evolution as a function of Fourier number during the charge and discharge process for different number of fins.

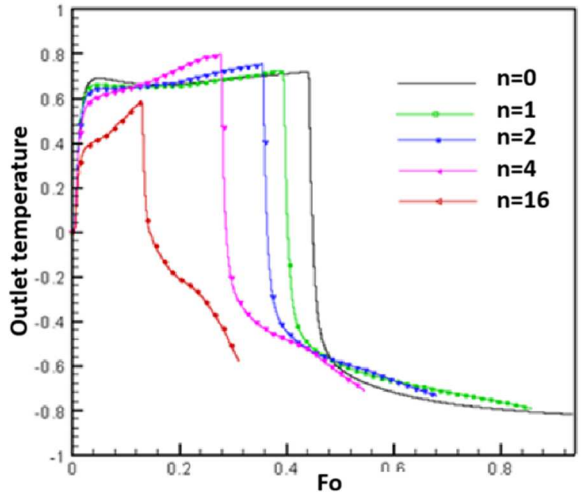

Fig. 38. Outlet temperature evolution as a function of Fourier number during the charge and discharge process for different number of fins.

A similar trend is observed for the partially charged cases (initial liquid fractions of 0.5, 0.75, and 0.9), with lower initial liquid fractions requiring proportionally shorter discharge times. The nearly linear evolution of the liquid fraction suggests that, after the initial stage of solidification, buoyancy-driven convection within the remaining liquid rapidly weakens as the solid layer grows. Consequently, heat transfer becomes increasingly dominated by conduction through the solid PCM, resulting in a nearly uniform solidification rate over most of the discharge process.

When solidification begins from partial melting, a second solidification front initiates its propagation from the left side of the cavity during the discharge phase. The relative solidification time, calculated as the ratio of the solidification time to the total cycle time, is shown in Fig. 36. This variation arises from the contribution of convection in accelerating the melting process, and the relative solidification time reaches its maximum for an initial liquid fraction of 0.6.

The incorporation of fins, increasing the exchange surface with the PCM, leads to an improvement in the overall melting time. The impact of the number of fins on the PCM's behavior during a charge-discharge cycle is investigated, as shown in Fig. 37, showcasing the liquid fraction's evolution for fin numbers equal to 0, 1, 2, 4, and 16. In all the studied cases, the discharge time is longer than the charge time, and the discharge rate remains relatively constant, primarily influenced by the number of fins. Figure 38 illustrates the variation of the outlet temperature with time. During the initial melting phase, the outlet temperature decreases with the addition of fins due to the enlarged heat exchange surface with the PCM. Conversely, during discharge, the outlet temperature exhibits a smoother variation, and its behavior strongly depends on the number of fins.

4. Conclusion

The present study presented a combined investigation of PCM melting and solidification in a fin-enhanced configuration using the Lattice Boltzmann Method coupled with the enthalpy approach. This framework enabled the simultaneous description of heat transfer, natural convection, and solid–liquid phase change while accounting for the effect of metallic fins as extended heat-transfer surfaces. Unlike studies focusing exclusively on melting or solidification, the present work considered both phases, thereby providing a more comprehensive assessment of the thermal behavior of the PCM system. We investigated the effect of the insertion of conducting fins on the improvement of thermal transfers in the phase change material (PCM). Impact of control parameters such as the size, number, and thickness of fins on the duration and performance of the heat system were conducted. According to the above discussions, the following conclusions can be drawn:

- In the case without fins, the presence of natural convection accelerates the melting process and the contribution of convection to the heat transfer within the PCM reduces significantly the charging time (PCM melting) by about 25%.
- The addition of fins to the LHTES system improves the melting time and increases the heat transfer by increasing the average storage power. The reduction in the complete melting time reaches 80% compared to no fin's arrangement. However, when the number of fins is greater than 12, this reduction remains practically constant.
- The discharge time is longer than the charge time, and the discharge speed remains relatively constant, primarily influenced by the number of fins. During the discharge phase, the outlet temperature undergoes a smoother variation, with its behavior significantly dependent on the number of fins.

Author Contributions

O. El Mhamdi and E. Semma defined the methodology, developed the code, validated the results and drafted the original paper. H. Faraji and M. El Alami participated in the validation of results and writing the final paper. The manuscript was written through the contribution of all authors. All authors discussed the results, reviewed, and approved the final version of the manuscript.

Acknowledgments

Not applicable.

Conflict of Interest

The authors declared no potential conflicts of interest concerning the research, authorship, and publication of this article.

Funding

The authors received no financial support for the research, authorship, and publication of this article.

Data Availability Statements

The datasets generated and/or analyzed during the current study are available from the corresponding author on reasonable request.

Nomenclature

C_p	Specific heat capacity [J/kg.K]	Ste	Stefan number
g	Gravity acceleration [m/s²]	X	Spacial position vector [m]
G	Particle distribution function for thermal field	t	Time [s]
C	Lattice speed [m/s]	T	Temperature [K]
F	Buoyancy [kg.m/s²]	u_r	Radial velocity component [m/s]
Fo	Fourrier number	u_z	Vertical velocity component [m/s]
f_l	Volume fraction of liquid	β	Thermal expansion coefficient [K^{-1}]
H	Total enthalpy [kJ/kg]	μ	Dynamic viscosity [Pa.s]
L	Height of the enclosure [m]	υ	Kinematic viscosity [m²/s]
L_f	Latent heat of melting [J/kg]	ρ	Mass density [kg/m³]
K	Thermal conductivity [W/mK]	ΔT	Temperature difference [K]
Nu	Nusselt number	Ω	Collision operator
Pr	Prandt number	ω	Weight function
Ra	Rayleigh number		

References

[1] Faraji, H., Benkaddour, A., Oudaoui, K., El Alami, M., Faraji, M., Emerging Applications of Phase Change Materials: A Concise Review of Recent Advances, *Heat Transfer*, 50, 2021, 1443–93.
[2] Arshad, A., Jabbal, M., Yan, Y., Darkwa, J., The Micro-/Nano-PCMs for Thermal Energy Storage Systems: A State of Art Review, *International Journal of Energy Research*, 43, 11, 2019, 5572–5620.
[3] Abhat, A., Low Temperature Latent Heat Thermal Energy Storage: Heat Storage Materials, *Solar Energy*, 30, 1983, 313–32.
[4] Faraji, H., El Alami, M., Arshad, A., Hariti, Y., Numerical Survey on Performance of Hybrid NePCM for Cooling of Electronics: Effect of Heat Source Position and Heat Sink Inclination, *Journal of Thermal Science and Engineering Applications*, 13, 2020, 1–30.
[5] Arshad, A., Jabbal, M., Faraji, H., Talebizadehsardari, P., Bashir, M. A., Yan, Y. Numerical Study of Nanocomposite Phase Change Material-Based Heat Sink for the Passive Cooling of Electronic Components, *Heat and Mass Transfer*, 2021, 1–15.
[6] Benkaddou, A., Faraji, M., Faraji, H., Numerical Study of the Thermal Energy Storage Behaviour of a Novel Composite PCM/Concrete Wall Integrated Solar Collector, *Materials Today: Proceedings*, 30, 2019, 905–8.
[7] Gounni, A., El Alami, M., Mabouk, M.T., Kheiri. A., Experimental Study of Thermal Performance of a Reduced Scale Cavity Equipped with Phase Change Material: Study of the Optimal Phase Change Material Layer Location, *Journal of Solar Energy Engineering, Transactions of the ASME*, 140, 2018.
[8] Berroug, F., Lakhal, E. K., El Omari, M., Faraji, M., El Qarnia, H., "Numerical Study of Greenhouse Nocturnal Heat Losses, *Journal of Thermal Science*, 20, 2011, 377–84.
[9] Agyenim, F., Hewitt, N., Eames, P., Smyth, M., A review of materials, heat transfer and phase change problem formulation for latent heat thermal energy storage systems (LHTESS), *Renewable and Sustainable Energy Reviews*, 14(2), 2010, 615-628.
[10] Mohamed, T., Arıcı, M., SelçukMert, M., Ajarostaghi, S.S.M., Niyas, H., Tunçbilek, E., Ismail, K.A.R., Younsi, Z., Benhouia, A.T., Mezaache, E., A Comprehensive Review of Micro/Nano Enhanced Phase Change Materials, *Journal of Thermal Analysis and Calorimetry*, 147, 2022, 3989-4016.
[11] Esapour, M., Hosseini, M. J., Ranjbarn A.A., Pahamli, Y., Bahrampoury, R., Phase Change in Multi-Tube Heat Exchangers, *Renewable Energy*, 85, 2016, 1017–25.
[12] Francis, A., Eames, P., Smyth, M., Heat Transfer Enhancement in Medium Temperature Thermal Energy Storage System Using a Multitube Heat Transfer Array, *Renewable Energy*, 35, 2010, 198–207.

[13] Mastani, J.M., Seddegh, S., Wang, X., Haghighat, F., Experimental Investigation of Multiple Tube Heat Transfer Enhancement in a Vertical Cylindrical Latent Heat Thermal Energy Storage System, *Renewable Energy*, 140, 2019, 234–44.
[14] Kousha N., Rahimi M., Pakrouh R., Bahrampoury R., Experimental Investigation of Phase Change in a Multitube Heat Exchanger, *Journal of Energy Storage*, 23 2019, 292–304.
[15] Majid, G., Hosseini, M.J., Rahimi. M., Bahrampoury, R., Nano-Enhancement of Phase Change Material in a Shell and Multi-PCM-Tube Heat Exchanger, *Journal of Energy Storage*, 22, 2019, 88–97.
[16] Changda, N., Liu, J., Deng, S., Effect of Geometric Parameter and Nanoparticles on PCM Melting in a Vertical Shell-Tube System, *Applied Thermal Engineering*, 184, 2021, 116290.
[17] Pahamli, Y., Hosseini, M. J., Ranjbar, A. A., Bahrampoury R., Effect of Nanoparticle Dispersion and Inclination Angle on Melting of PCM in a Shell and Tube Heat Exchanger, *Journal of the Taiwan Institute of Chemical Engineers*, 81, 2017, 316–34.
[18] Mayilvelnathan, V., ValanArasu, A., Experimental Investigation on Thermal Behavior of Graphene Dispersed Erythritol PCM in a Shell and Helical Tube Latent Energy Storage System, *International Journal of Thermal Sciences*, 155, 2020, 106446.
[19] Al-Mudhafar Ahmed, H.N., Andrzej, F., Kowski, N., Franck C.G.A. Nicolleau, Enhancing the Thermal Performance of PCM in a Shell and Tube Latent Heat Energy Storage System by Utilizing Innovative Fins, *Energy Reports*, 7, 2021, 120–26.
[20] Hongtao, X., Wang, N., Zhang, C., Qu, Z., Cao, M., Optimization on the Melting Performance of Triplex-Layer PCMs in a Horizontal Finned Shell and Tube Thermal Energy Storage Unit, *Applied Thermal Engineering*, 176, 2020, 115409.
[21] Kaan, Y.O., Avci,M., Aydin, O., Melting and Solidification of PCM in a Tube-in-Shell Unit: Effect of Fin Edge Lengths' Ratio, *Journal of Energy Storage*, 24, 2019, 100802.
[22] Dekhil M.A., Voguelin, J., Tala, S., Bulliard-Sauret, O., Bougeard, D., Numerical Analysis of the Performance Enhancement of a Latent Heat Storage Shell and Tube Unit Using Finned Tubes during Melting and Solidification, *Applied Thermal Engineering*, 192, 2021, 116866.
[23] Turan, O., Yiğit, S., Chakraborty, N, Effects of wall heating on laminar mixed convection in a cylindrical enclosure with a rotating end wall, *International Journal of Thermal Sciences*, 131, 2018, 80–93.
[24] Huang, R., Wu, H., Cheng, P., A new lattice Boltzmann model for solid–liquid phase change, *International Journal of Heat and Mass Transfer*, 59, 2013, 295-301,
[25] Huang, R., Wu, H.,. A modified multiple-relaxation-time lattice Boltzmann model for convection–diffusion equation, *Journal of Computational Physics*, 274, 2014, 50-63.
[26] Huang, R., Wu, H., Phase interface effects in the total enthalpy-based lattice Boltzmann model for solid–liquid phase change, *Journal of Computational Physics*, 294, 2015, 346–362.
[27] Wang, Y., Shu, C., Teo, C.J., A fractional step axisymmetric lattice Boltzmann flux solver for incompressible swirling and rotating flows, *Computers & Fluids*, 96, 2014, 204–214.
[28] Kumar, R., Kalam, M., Laminar thermal convection between vertical coaxial isothermal cylinders, *International Journal of Heat and Mass Transfer*, 34, 1991, 513.
[29] Venkatachalappa, M., Sankar, M. and Natarajan, A.A., Natural convection in an annulus between two rotating vertical cylinders, *Acta Mechanica*, 147, 2001, 173–196.
[30] Chen Z., Shua C., Tan D., Three-dimensional simplified and unconditionally stable lattice Boltzmann method for incompressible isothermal and thermal flows, *Physics of Fluids*, 29, 2017, 053601.
[31] Li, D., Ren, Q., Tong, Z-X., He, Y-L., Lattice Boltzmann models for axisymmetric solid–liquid phase change, *International Journal of Heat and Mass Transfer*, 112, 2017, 795-804.
[32] El Mhamdi, O., Addakiri, S., Semma, E., El Alami, M., Study of A Thermal Energy Storage System Using the Lattice Boltzmann Method, *E3S Web of Conferences*, 321, 2021, 04003.

ORCID iD

Oussama El Mhamdi https://orcid.org/0000-0002-2548-465X
Elalami Semma https://orcid.org/0000-0001-6145-6122
Hamza Faraji https://orcid.org/0000-0003-2792-4986
Mustapha El Alami https://orcid.org/0000-0001-5020-9388

How to cite this article: El Mhamdi, O., Semma, E., Faraji, H., El Alami, M. Numerical Investigation of Heat Transfer Enhancement for Finned Double Tube Latent Heat Thermal Energy Storage using Lattice Boltzmann Method, *J. Appl. Comput. Mech.*, xx(x), 2026, 1–22. https://doi.org/10.22055/jacm.2026.49250.5837